Electronic Supplementary Information (ESI)

A densely decorated disubstituted ferrocene as a redox, chromogenic and fluorescent ion-pair recognition receptor.

María del Carmen González, Francisco Otón, Arturo Espinosa, Alberto Tárraga and Pedro Molina.**

Departamento de Química Orgánica, Facultad de Química Campus de Espinardo, Universidad de Murcia, E-30100 Murcia, Spain. Fax: +34 868 884 149; Tel: +34 868 887 496;

Table of contents

Description of computed structure for receptor 1.

Detailed description of the ^{1}H NMR titration with metals.

Experimental Section.

General Comments.- Melting points were determined on a hot-plate melting point apparatus and are uncorrected. ^{1}H and ^{13}C spectra were recorded on a 300, or 400 MHz apparatus. The following abbreviations have been used for stating the multiplicity of the signals: s (singlet), d (doublet), t (triplet), pt (pseudotriplet), q (quaternary carbon). Chemical shifts refer to signals of tetramethylsilane in the case of ^{1}H and ^{13}C spectra. CV and OSWV techniques were performed with a conventional three-electrode configuration consisting of platinum working and auxiliary electrodes and a Ag/AgCl reference electrode. The experiments were carried out with a 5×10^{-4} M solution of sample in an adequate solvent containing 0.1 M $(n\text{-}C_4H_9)_4NPF_6$ ($(TBA)PF_6$) as the supporting electrolyte. All the potential values reported are relative to the ferrocene couple at room temperature. Deoxygenation of the solutions was achieved by bubbling nitrogen for at least 10 min, and the working electrode was cleaned after each run. The cyclic voltammograms were recorded with a scan rate increasing from 0.05 to 1.00 V s^{-1}, while the OSWV curves were recorded at a scan rate of 100 mV s^{-1} with a pulse height of 10 mV and a step time of 50 ms. Typically, receptor (5×10^{-4} M) was dissolved in the appropriate solvent (5 mL) and TBAHP (base electrolyte) (0.1 M) added. The guest under investigation was then added as a 2.5×10^{-2} M solution in the appropriate solvent using a microsyringe while the cyclic voltammetric properties of the solution were monitored. Fc was used as an external and/or internal reference both for potential calibration and for reversibility criteria. Under similar conditions, Fc has E = 0.39 V vs SCE and the anodic−cathodic peak separation is 67 mV. UV-vis spectra were carried out in a UV-vis-NIR spectrophotometer using a dissolution cell of 10 mm path. The samples were solved in CH_3CN / CH_2Cl_2 (4:1, $c = 3x10^{-5}$ M) and the spectra were recorded with the spectra backqround corrected before and after of the sequential additions of different aliquots of cations/anions in CH_3CN ($c = 2.5x10^{-2}$ M). Fluorescence spectra were carried out in a fluorescence spectrophotometer using a fluorescence cell 10 mm ($c = 1.5x10^{-5}$ M in CH_3CN / CH_2Cl_2 4:1), as it is stated in the corresponding figure captions. Before recording the spectra, the samples were deoxygenated, to remove fluorescence quenching via oxygen, by bubbling nitrogen for at least 10 min. All the spectra were recorded before and after the sequential additions of different aliquots of a solution of cations/anions in CH_3CN ($c = 2.5x10^{-2}$ M). Quantum yield values were measured with respect to anthracene as the standard (Φ = 0.27 ± 0.01) using the equation $\Phi_x/\Phi_s = (S_x/S_s)\ [(1 - 10^{-As})/(1 - 10^{-Ax})](n_s^2/n_x^2)$, where x and s indicate the unknown and standard solutions, respectively, F is the quantum yield, S is the area under the emission curve, A is the absorbance at the excitation wavelength, and n is the refractive index. For the calculation of the association constants, the corresponding titrations were carried out 3 or 4 times in order to test the reliability of the results and the calculation of the associated error that are included in a table below.

Computational Details.- Quantum chemical calculations were performed with the ORCA electronic structure program package.[1] Geometry optimizations were run with tight convergence criteria[2] using the B3LYP[3] functional together with the new efficient RIJCOSX algorithm[4] and the def2-TZVP basis set.[5] In all optimizations and energy evaluations, the latest Grimme's semiempirical atom-pair-wise correction, accounting for the major part of the contribution of dispersion forces to the energy, was included.[6] Solvent effects (acetonitrile) were taken into account via the COSMO solvation model.[7] From these geometries all reported data were obtained by means of single-point (SP) calculations using the same functional as well as the more polarized def2-TZVPP[4,8] basis set. Bond strengths were characterized by the Wiberg Bond Index (WBI).[9] The topological analysis of the electronic charge density, ρ(**r**), within Bader's Atoms-In-Molecules (AIM) methodology[10] was conducted using the AIM2000 software[11] and the wavefunctions (electron density) generated with the Gaussian09 software package.[12] Reported energies are uncorrected for the zero-point vibrational term.

---

[1] ORCA - An *ab initio*, DFT and semiempirical SCF-MO package. Written by F. Neese, Max Planck Institute for Bioinorganic Chemistry, D-45470 Mülheim/Ruhr, 2012. Version 2.9.1. Web page: http://www.mpibac.mpg.de/bac/logins/neese/description.php. F. Neese, *WIREs Comput Mol Sci* **2012**, *2*, 73–78.

[2] Looser criteria were used with complex $[\mathbf{2}_2{\cdot}(H_2PO_4)_2]^{2-}$.

[3] (a) A. D. Becke, *J. Chem. Phys.*, **1993**, *98*, 5648-5652. (b) C.T. Lee, W.T. Yang and R.G. Parr, *Phys. Rev. B* **1988**, *37*, 785-789.

[4] F. Neese, F. Wennmohs, A. Hansen, U. Becker, *Chem. Phys.*, **2009**, *356*, 98-109.

[5] F. Weigend, R. Ahlrichs, *Chem. Phys.*, **2005**, *7*, 3297-3305.

[6] S. Grimme, J. Antony, S. Ehrlich, H. Krieg, *J. Chem. Phys.*, **2010**, *132*, 154104.

[7] (a) A. Klamt, G. Schüürmann, *J. Chem. Soc. Perkin Trans. 2,* **1993**, *220*, 799-805; (b) A. Klamt, *J. Phys. Chem.* **1995**, *99*, 2224-2235.

[8] A. Schäfer, C. Huber, R. Ahlrichs, *J. Chem. Phys.*, 1994, *100*, 5829-5835; basis sets may be obtained from the Basis Set Exchange (BSE) software and the EMSL Basis Set Library: https://bse.pnl.gov/bse/portal. D. Feller, *J. Comp. Chem*., 1996, *17*, 1571-1586.

[9] K. Wiberg, *Tetrahedron* **1968**, *24*, 1083-1096.

[10] (a) R. F. W. Bader, in *Atoms in Molecules: A Quantum Theory*, Oxford University Press, Oxford, 1990. (b) R. F. W. Bader, *Chem. Rev.*, 1991, *91*, 893-928. (c) C. F. Matta, R. J. Boyd, in *The Quantum Theory of Atoms in Molecules*; C. F. Matta, R. J. Boyd, Eds., Wiley-VCH: New York, 2007; pp 1-34.

[11] (a) AIM2000 v. 2.0, designed by F. W. Biegler-König, and J. Schönbohm, 2002. Home page http://www.aim2000.de/. F. Biegler-König, J. Schönbohm and D. J. Bayles, *Comp. Chem.* **2001**, *22*, 545-559. (b) F. Biegler-König, J. Schönbohm, *J. Comp. Chem.*, **2002**, *23*, 1489-1494.

[12] Gaussian 09, Revision A.02, M. J. Frisch, G. W. Trucks, H. B. Schlegel, G. E. Scuseria, M. A. Robb, J. R. Cheeseman, G. Scalmani, V. Barone, B. Mennucci, G. A. Petersson, H. Nakatsuji, M. Caricato, X. Li, H. P. Hratchian, A. F. Izmaylov, J. Bloino, G. Zheng, J. L. Sonnenberg, M. Hada, M. Ehara, K. Toyota, R. Fukuda, J. Hasegawa, M. Ishida, T. Nakajima, Y. Honda, O. Kitao, H. Nakai, T. Vreven, J. A. Montgomery, Jr., J. E. Peralta, F. Ogliaro, M. Bearpark, J. J. Heyd, E. Brothers, K. N. Kudin, V. N. Staroverov, R. Kobayashi, J. Normand, K. Raghavachari, A. Rendell, J. C. Burant, S. S. Iyengar, J. Tomasi, M. Cossi, N. Rega, N. J. Millam, M. Klene, J. E. Knox, J. B. Cross, V. Bakken, C. Adamo, J. Jaramillo, R. Gomperts, R. E. Stratmann, O. Yazyev, A. J. Austin, R. Cammi, C. Pomelli, J. W. Ochterski, R. L. Martin, K. Morokuma, V. G. Zakrzewski, G. A. Voth, P. Salvador, J. J. Dannenberg, S. Dapprich, A. D. Daniels, Ö. Farkas, J. B. Foresman, J. V. Ortiz, J. Cioslowski, D. J. Fox, Gaussian, Inc., Wallingford CT, 2009.

Preparation of 1-[(4-Pyrenyl-1,2,3-triazol-1-yl)]-1´-[3-coumarincarbonil]-aminoferrocene, 1.

In a 100 ml round flask equipped with a reflux under nitrogen atmosphere, 0.4 ml of thionyl chloride (5.5 mmol) were added over 0.029 g (0.152 mmol) of 3-coumarincarboxilic acid. Then the mixture is stirred at 100ºC for 2.5 hours. After this time the remaining thionyl chloride is removed under vacuum and 0.05 g (0.107 mmol) of 1-(4-(1-pyrenyl)-1,2,3-triazol-1-yl)-1´-aminoferrocene and 10 ml of THF were added to the reaction under nitrogen atmosphere and stirred at room temperature for 3 hours. Afterwards, solvent is removed under vacuum and the resulting solid is washed with dichloromethane and chromatographed in CH_2Cl_2/AcOEt 9:1 (R_f = 0.6) giving a dark red solid (0.056 g, 82% yield).

M.p. 240 °C (d); δ_H (400 MHz; CD_2Cl_2; Me_4Si) 9.80 (s, 1H, 13), 8.98 (d, 1H, ^3J = 9.3 Hz, 24), 8.23 (s, 1H, 17), 8.18 (d, 1H, ^3J = 7.6 Hz, 31 or 33) 8.17 (d, 1H, ^3J = 8 Hz, 23), 8.16 (d, 1H, ^3J = 7.6 Hz, 31 or 33), 8.11 (d, 1H, ^3J = 0.6 Hz, 41), 8.07 (d, 1H, ^3J = 9.3 Hz, 25), 8.03 (t, 1H, ^3J = 7.6 Hz, 32), 8.02 (d, 1H, ^3J = 8.0 Hz, 22), 8.01 (d, 1H, ^3J = 8.9 Hz, 29 or 30), 7.92 (d, 1H, ^3J = 8.9 Hz, 29 or 30) 6.52 (ddd, 1H, ^3J = 8.3 Hz, ^3J = 7.6 Hz, ^4J = 1.6 Hz, 44), 6.43 (dd, 1H, ^3J = 7.6 Hz, ^4J = 1.6 Hz, 42) 6.25 (ddd, 1H, ^3J = 8.3 Hz, ^4J = 1 Hz, ^4J = 0.6 Hz, 45) 6.21 (td, 1H, ^3J = 7.6 Hz ^4J = 1 Hz, 43), 5.19 (pt, 2H, Fc), 5.04 (pt, 2H, Fc), 4.40 (pt, 2H, Fc), 4.21 (pt, 2H, Fc); δ_C (101 MHz; CD_2Cl_2) 161.6 (q, CO, 37), 160.0 (q, CO, 34), 158.3 (q, 36), 153.4 (q), 147.7 (CH, 41), 147.51 (q, 16), 132.8 (CH, 44), 131.7 (q), 131.3 (q), 131.1 (q), 128.5 (CH, 42), 128.4 (CH, 25), 127.9 (CH, 29 or 30), 127.7 (q), 127.5 (CH, 29 or 30), 126.4 (CH, 22) 126.3 (CH, 31 or 33), 125.6 (CH, 31 or 33), 125.4 (CH, 23), 125.3 (CH, 24), 125.1 (CH, 32), 124.8 (q), 124.6 (q), 123.9 (CH, 43) 121.9 (CH, 17), 117.3 (q, 38), 116.9 (q, 40), 115.2 (CH, 45), 96.6 (q, Fc), 95.0 (q, Fc), 67.4 (CH, Fc), 66.5 (CH, Fc), 62.9 (CH, Fc), 62.5 (CH, Fc); ν_{max} (CH_2Cl_2)/cm^{-1}: 3583, 2953, 2919, 2849, 1710, 1698, 1652, 1605, 1548, 1453, 1385, 1360, 1275, 1225, 1198, 1157, 1026, 962, 874, 845, 830, 810; m/z (ESI) 640 (100, M^+); Anal. Calc. for $C_{38}H_{24}FeN_4O_3$: C, 71.26; H, 3.78; N, 8.75. Found: C, 71.34; H, 3.82; N, 8.72.

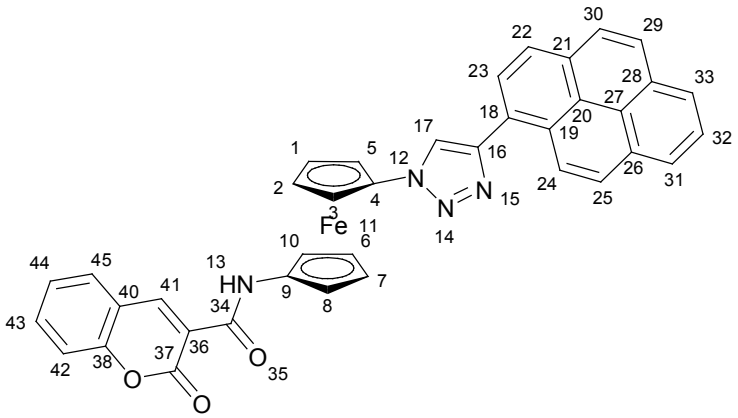

Figure S1. Number scheme for the atoms of the receptor **1**.

Figure S2. NMR spectra of **1**.

^{1}H NMR (CD_2Cl_2, 400MHz).

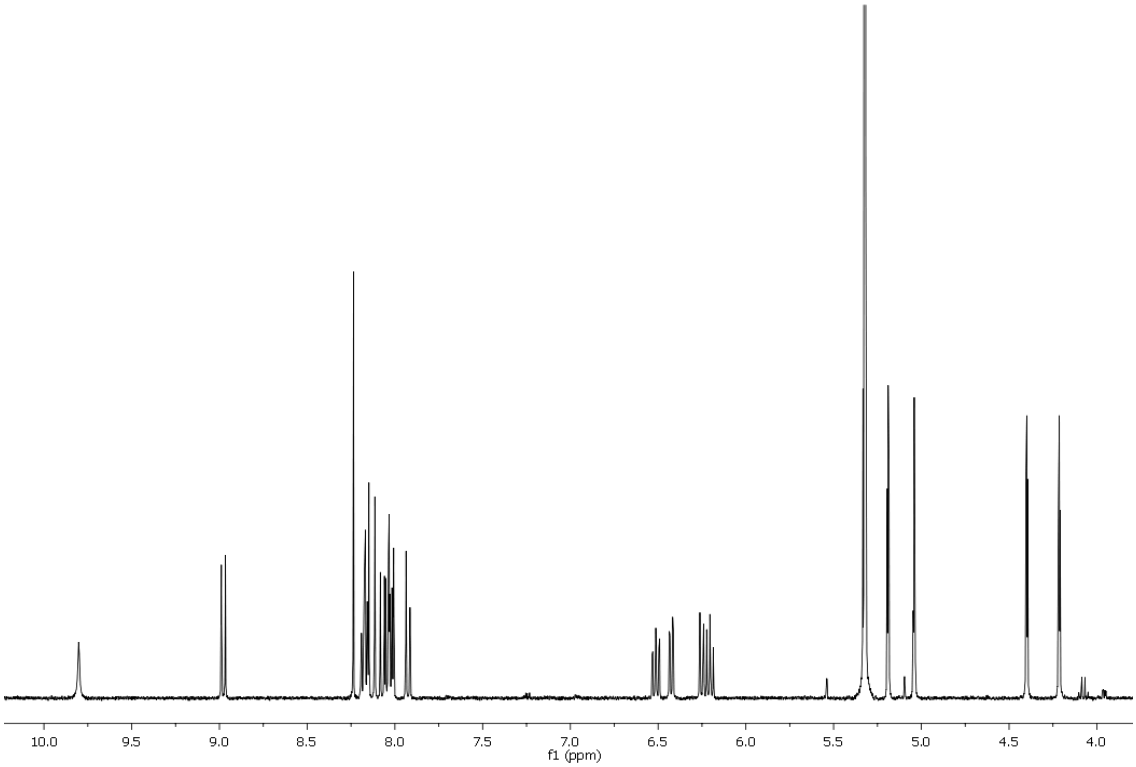

^{13}C NMR (CD_2Cl_2, 101MHz).

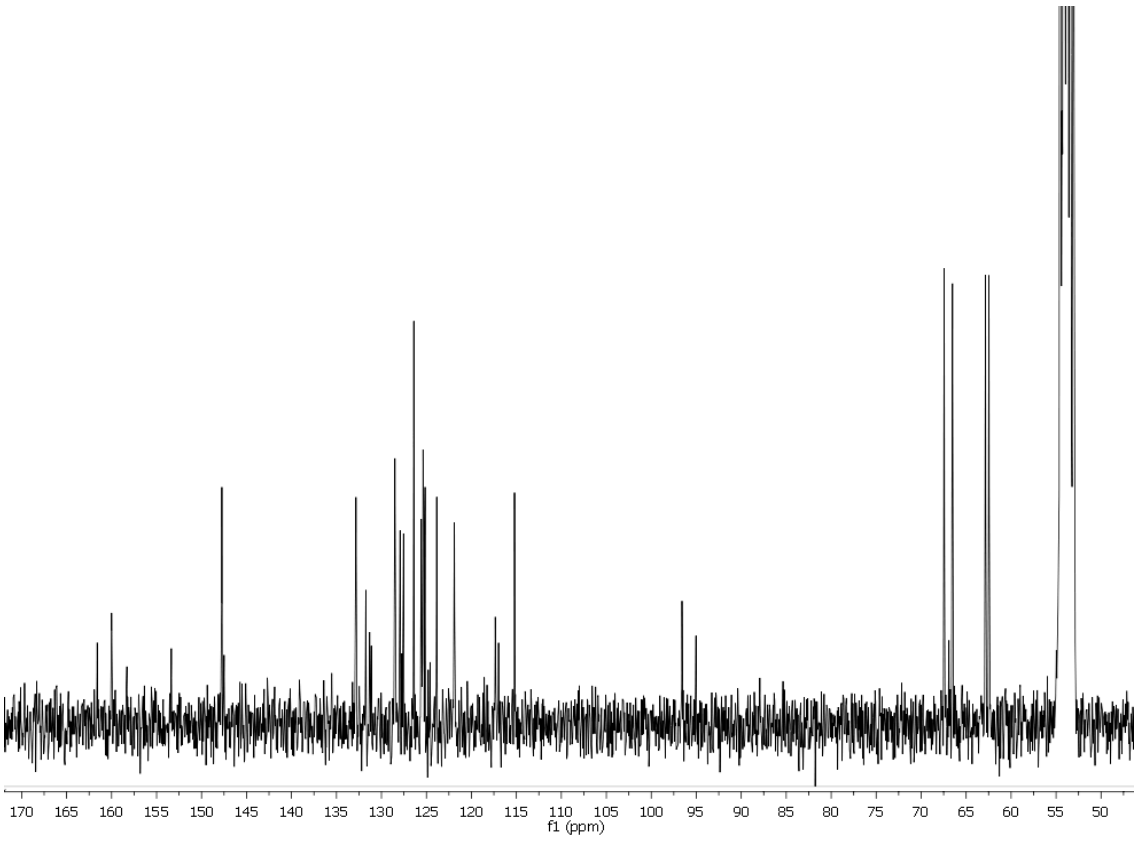

^{1}H-^{1}H COSY NMR (CD_2Cl_2, 400MHz).

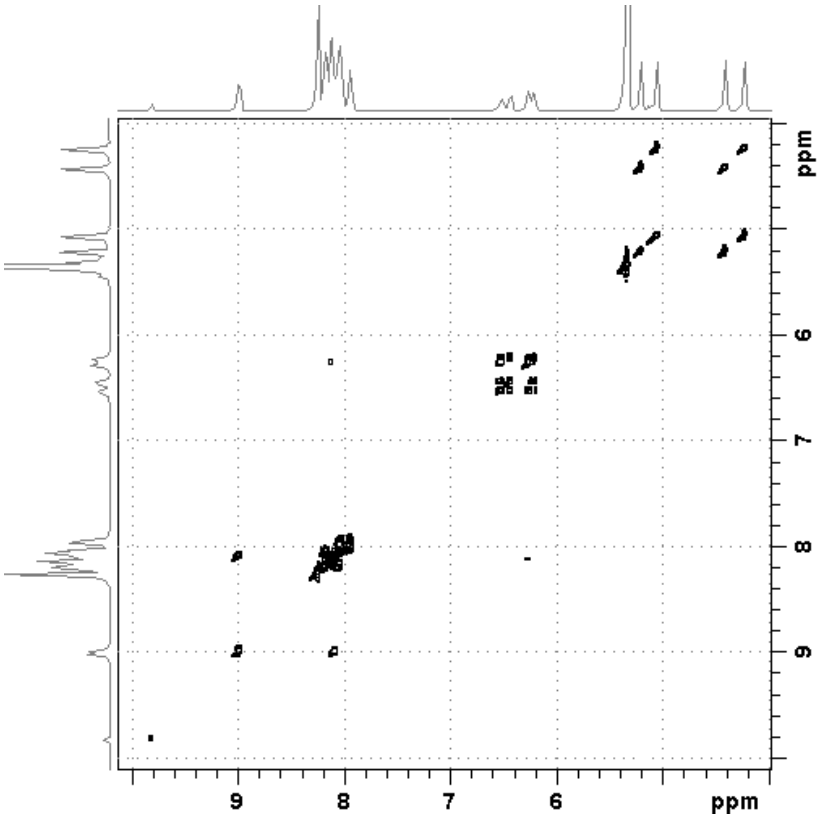

^{1}H-^{13}C HMQC NMR (CD_2Cl_2, 400MHz).

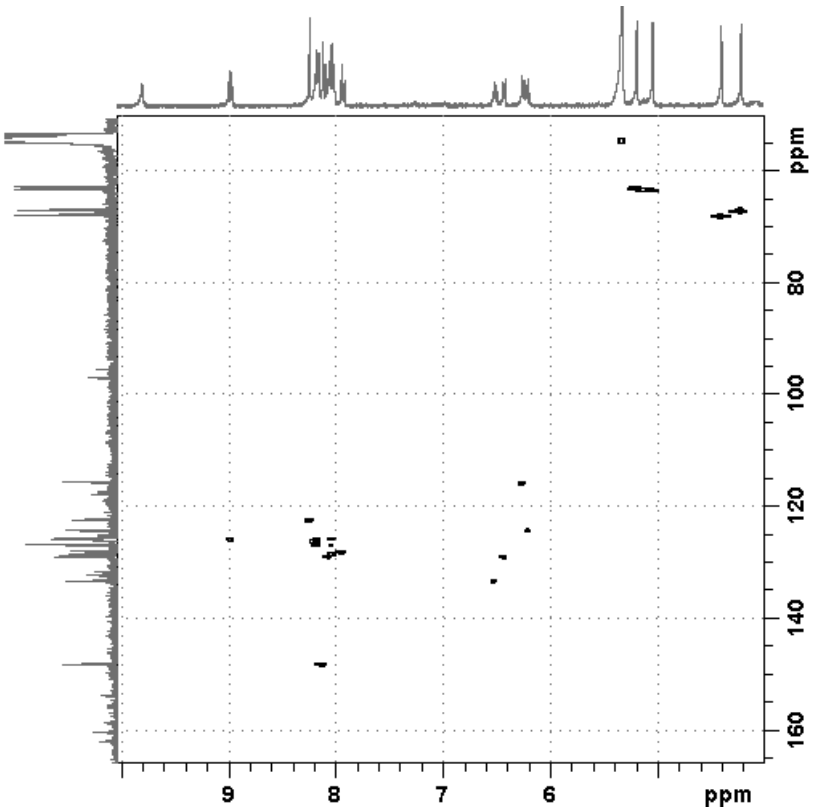

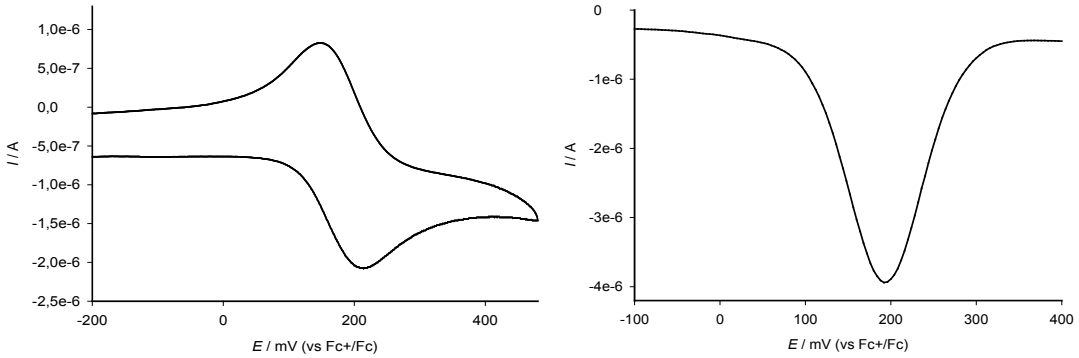

Figure S3. CV (left) and OSWV (right) of compound **1** in CH_3CN / CH_2Cl_2 (4:1, c = $5 \cdot 10^{-4}$ M) with 0.1 M of TBAHP as supporting electrolyte.

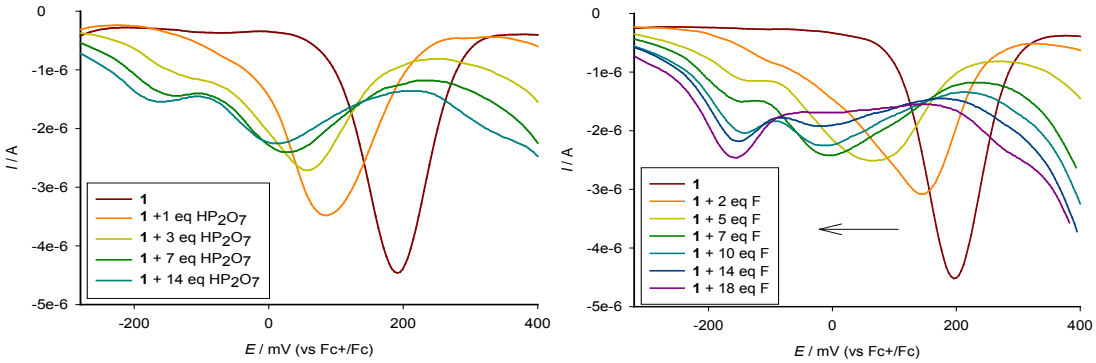

Figure S4. OSWV of the titration of compound **1** in CH_3CN / CH_2Cl_2 (4:1, c = $5 \cdot 10^{-4}$ M) with increasing amounts of $HP_2O_7^{-3}$ (left) and F^- (right) (supporting electrolyte, c = 0.1 M of TBAHP).

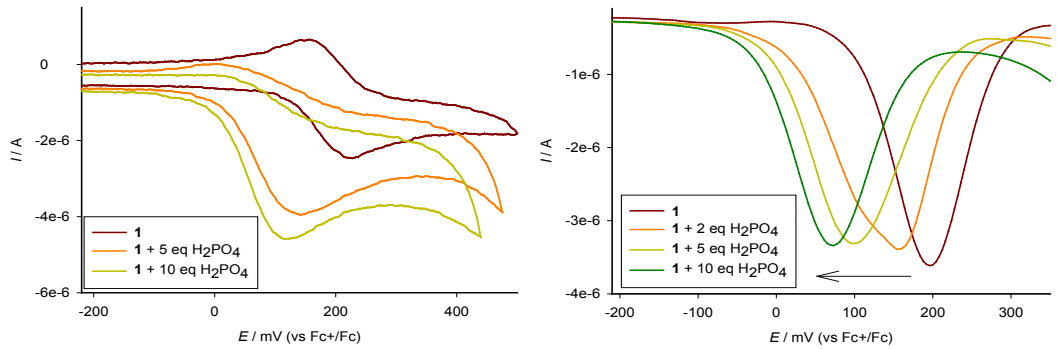

Figure S5. CV (left) and OSWV (right) of the titration of compound **1** in CH_3CN / CH_2Cl_2 (4:1, c = $5 \cdot 10^{-4}$ M) with increasing amounts of $H_2PO_4^-$ (supporting electrolyte, c = 0.1 M of TBAHP).

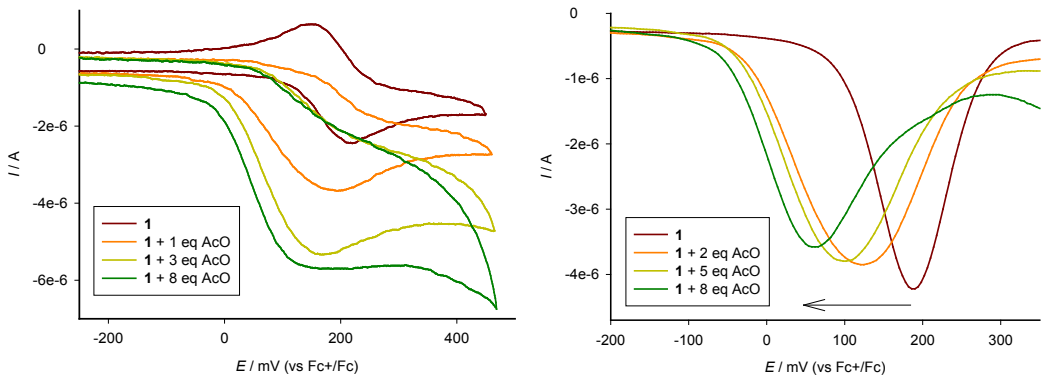

Figure S6. CV (left) and OSWV (right) of the titration of compound **1** in CH_3CN / CH_2Cl_2 (4:1, $c = 5 \cdot 10^{-4}$ M) with increasing amounts of AcO^- (supporting electrolyte, c = 0.1 M of TBAHP).

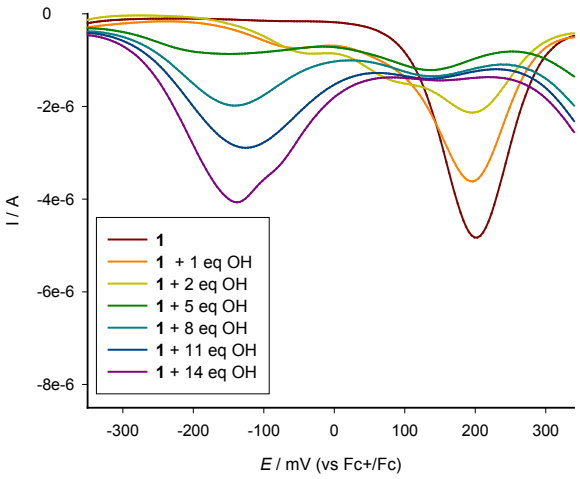

Figure S7. OSWV of the titration of compound **1** in CH_3CN / CH_2Cl_2 (4:1, $c = 5 \cdot 10^{-4}$ M) with increasing amounts of OH^- (supporting electrolyte, c = 0.1 M of TBAHP).

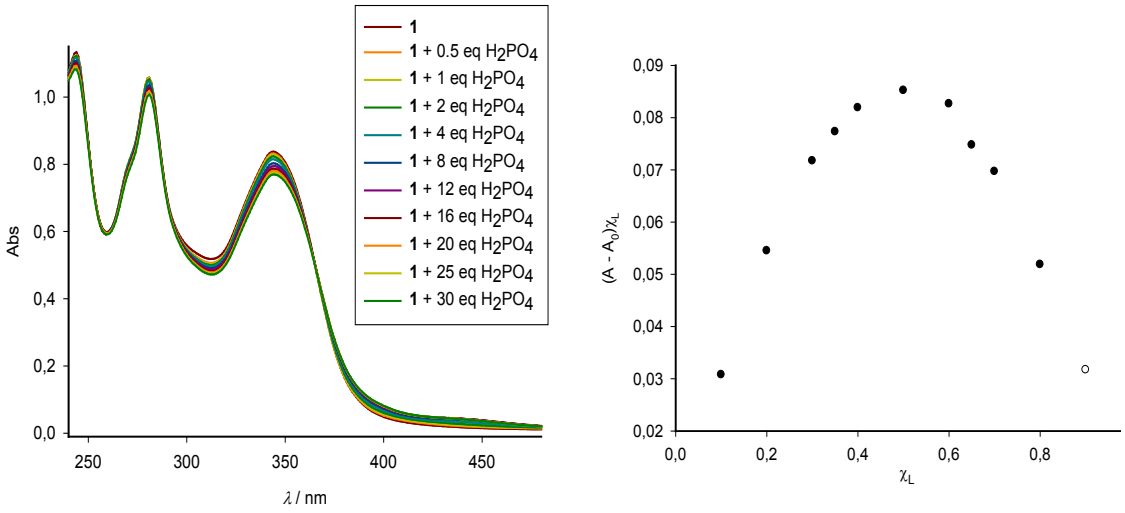

Figure S8. UV-Vis titration of compound **1** in CH_3CN / CH_2Cl_2 (4:1, $c = 3 \cdot 10^{-5}$ M) upon addition of $H_2PO_4^-$ from 0 to 30 equiv and Job´s plot showing a 1:1 stoichiometry. The total [**1**] + [A^-] = $3 \cdot 10^{-5}$ M.

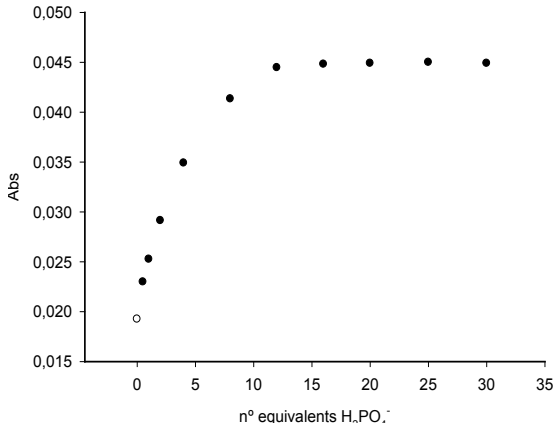

Figure S9. Binding profile of the titration of compound **1** in CH_3CN / CH_2Cl_2 (4:1, $c = 3 \cdot 10^{-5}$ M) with $H_2PO_4^-$ measured at 425 nm.

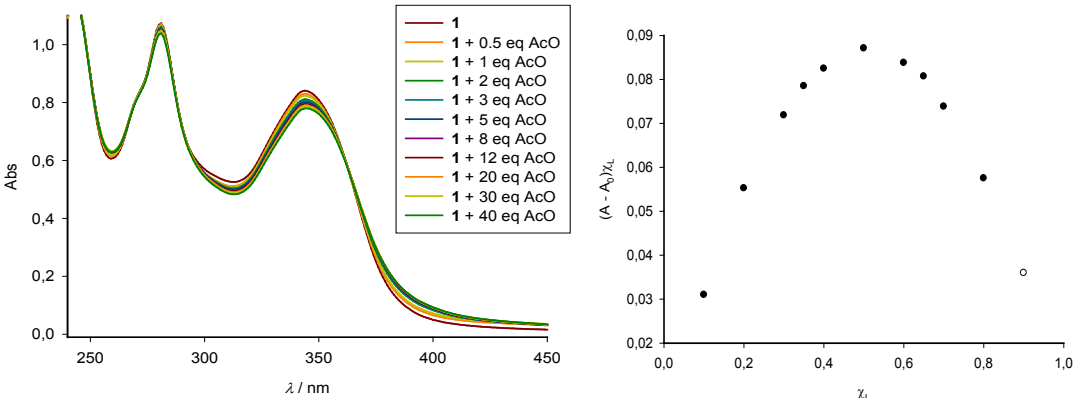

Figure S10. UV-Vis titration of compound **1** in CH_3CN / CH_2Cl_2 (4:1, $c = 3 \cdot 10^{-5}$ M) upon addition of AcO^- from 0 to 40 equiv and Job´s plot showing a 1:1 stoichiometry. The total [**1**] + [A^-] = $3 \cdot 10^{-5}$ M.

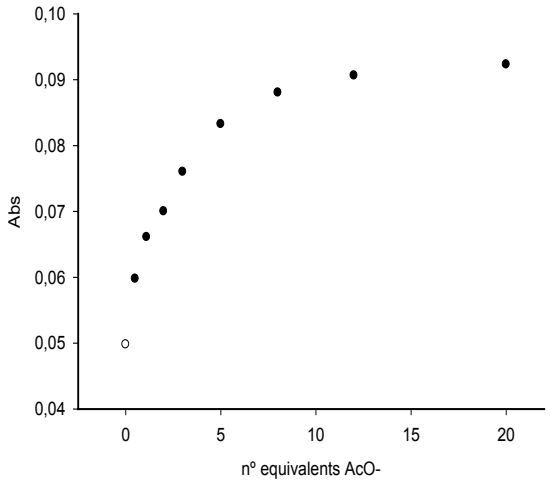

Figure S11. Binding profile of the titration of compound **1** in CH_3CN / CH_2Cl_2 (4:1, $c = 3 \cdot 10^{-5}$ M) with AcO^- measured at 425 nm.

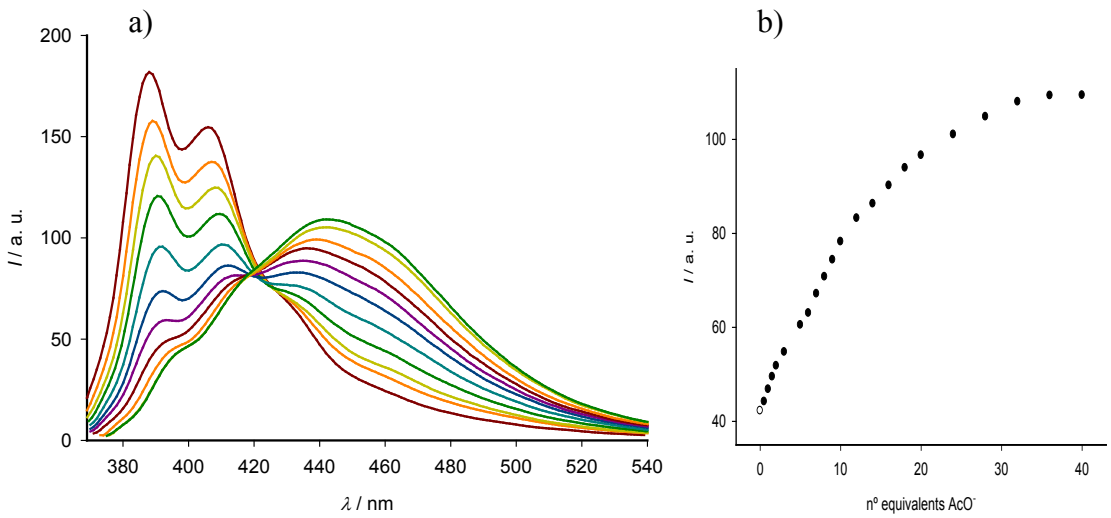

Figure S12. a) Fluorescence titration of compound **1** (λ_{exc} = 345 nm) in CH_3CN / CH_2Cl_2 (4:1) ($c = 1.5 \cdot 10^{-5}$ M) upon addition of increasing amounts of AcO^-. b) Binding profile measured at 443 nm.

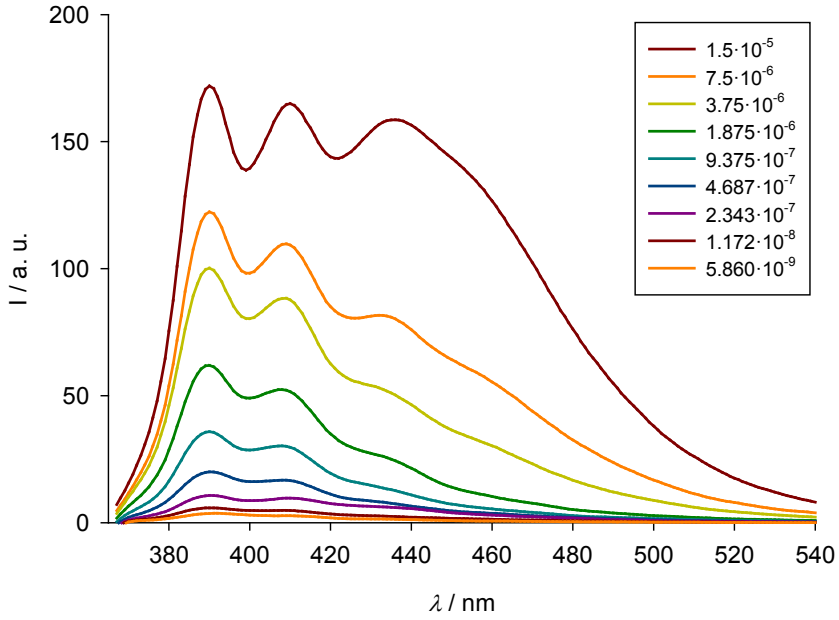

Figure S13. Decreasing of the excimer band of [**1**·$H_2PO_4^-$] (5 equiv of $H_2PO_4^-$) upon successive dilutions of the complex.

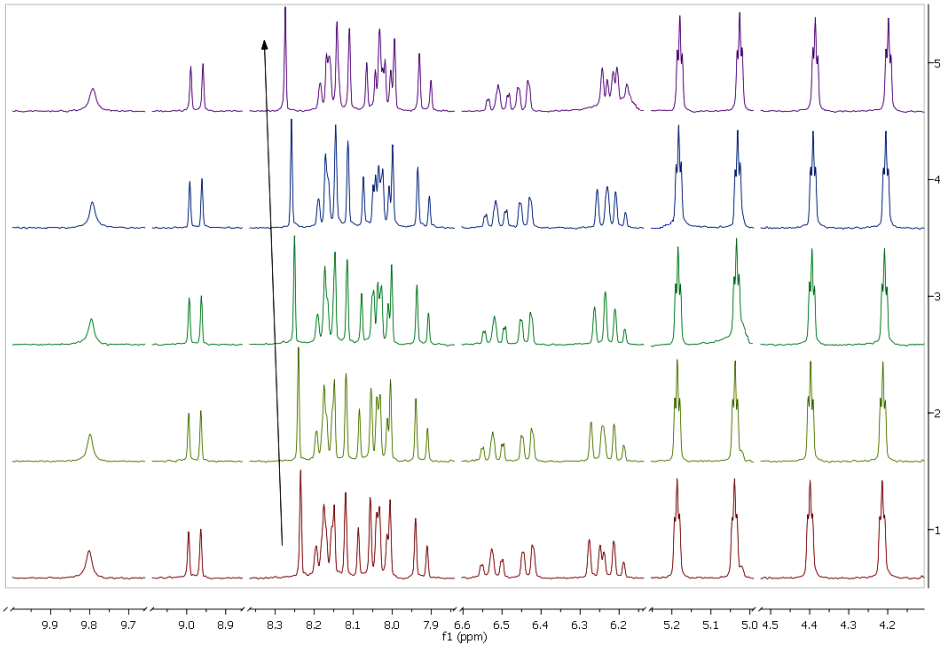

Figure S14. Changes of the ^{1}H-NMR spectra of **1** upon addition of 0 (bottom), 1, 5, 10 and 15 (top) equivalents of $H_2PO_4^-$.

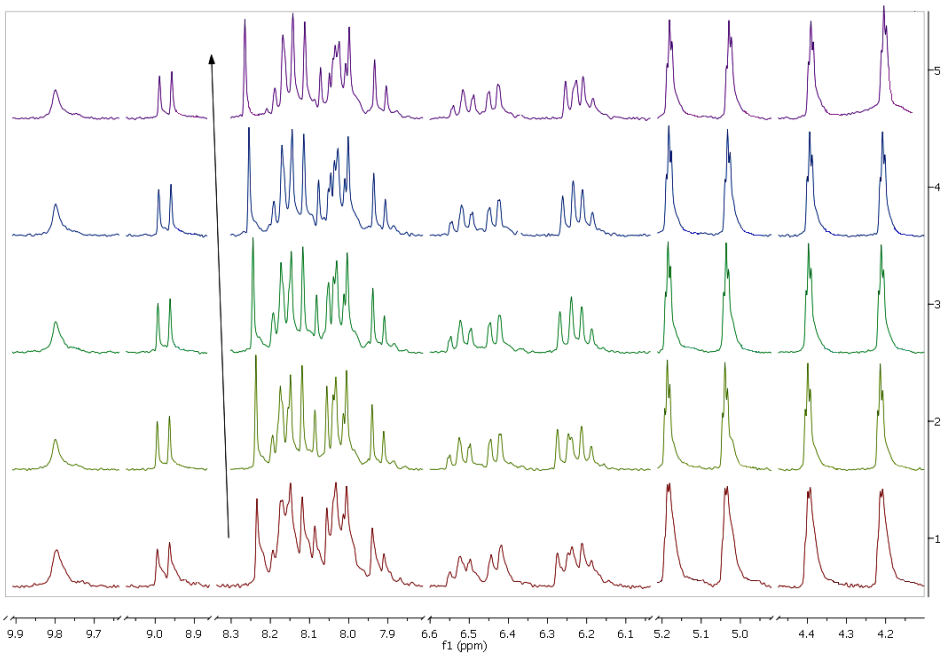

Figure S15. Changes of the ^{1}H-NMR spectra of **1** upon addition of 0 (bottom), 1, 5, 10 and 15 (top) equivalents of AcO^-.

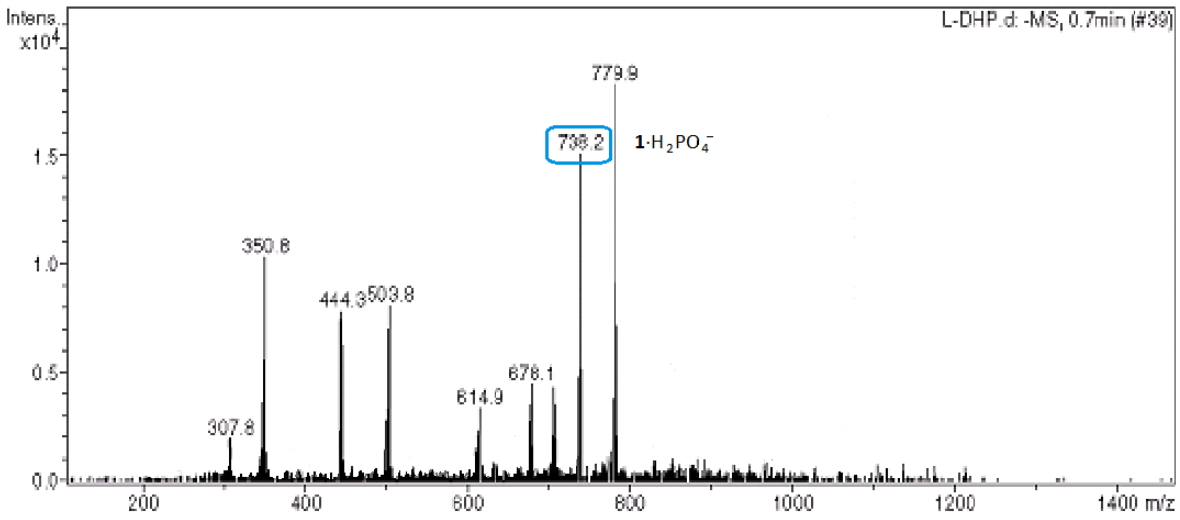

Figure S16. ESI-MS of the complex formed between receptor **1** and $H_2PO_4^-$.

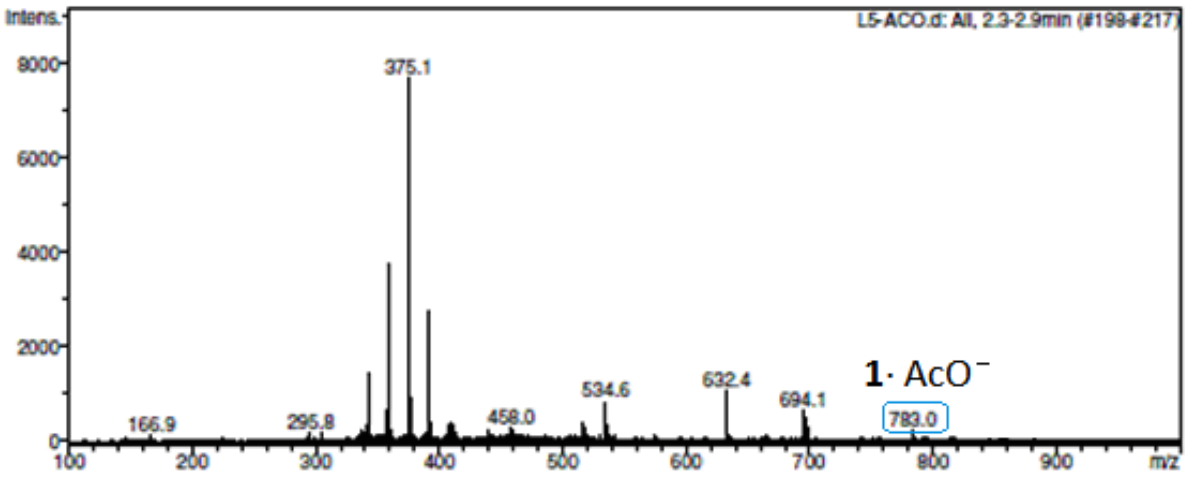

Figure S17. ESI-MS of the complex formed between receptor **1** and AcO^-.

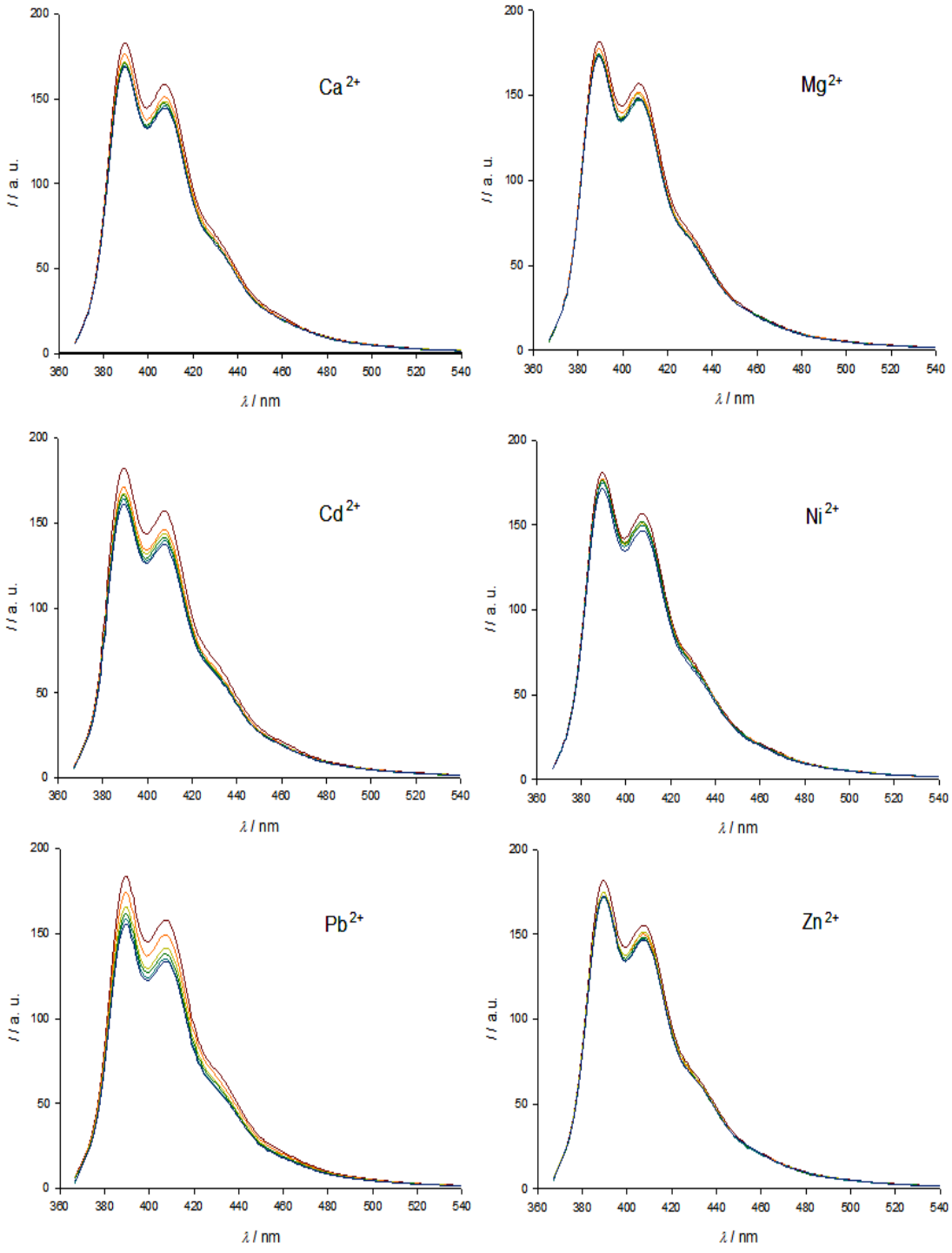

Figure S18. Fluorescence titrations of compound **1** in CH_3CN / CH_2Cl_2 (4:1, c = $1.5 \cdot 10^{-5}$ M) upon addition of a set of metal cations from 0 to 30 equiv.

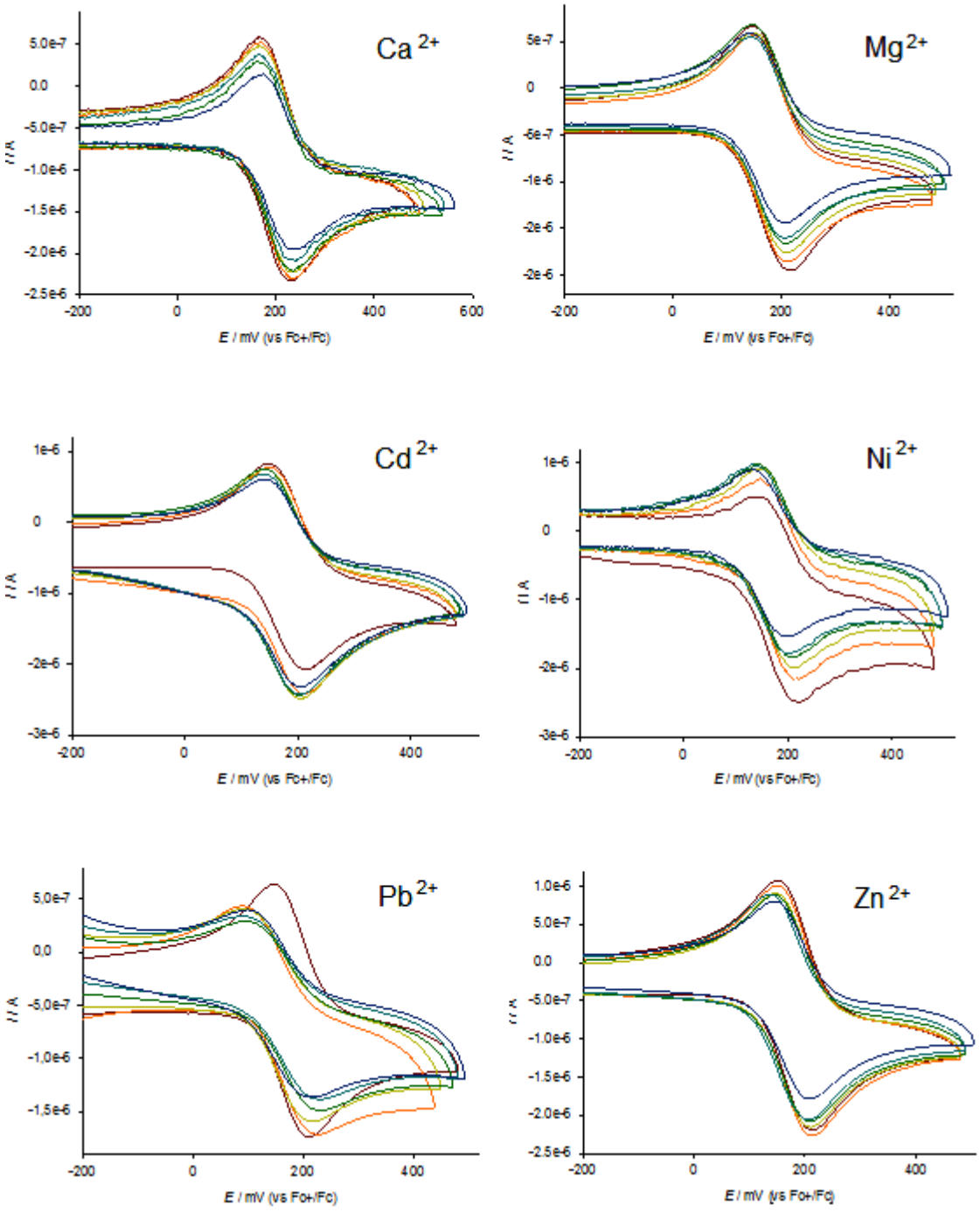

Figure S19. CV of the titrations of compound **1** in CH_3CN / CH_2Cl_2 (4:1, $c = 5 \cdot 10^{-4}$ M) with increasing amounts of a set of metal cations (supporting electrolyte, $c = 0.1$ M of TBAHP).

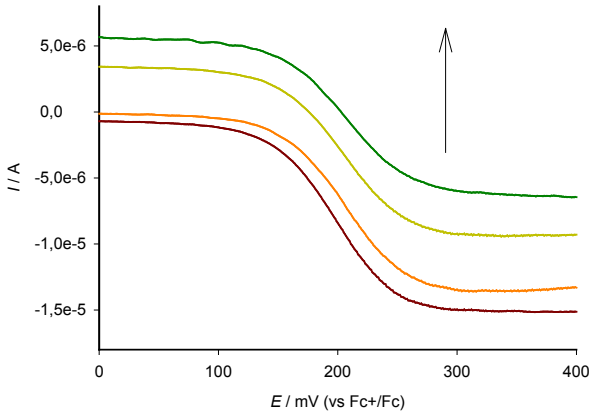

Figure S20. LV of the titration of compound **1** in CH_3CN / CH_2Cl_2 (4:1, $c = 5 \cdot 10^{-4}$ M) with increasing amounts of Hg^{2+} (supporting electrolyte, $c = 0.1$ M of TBAHP).

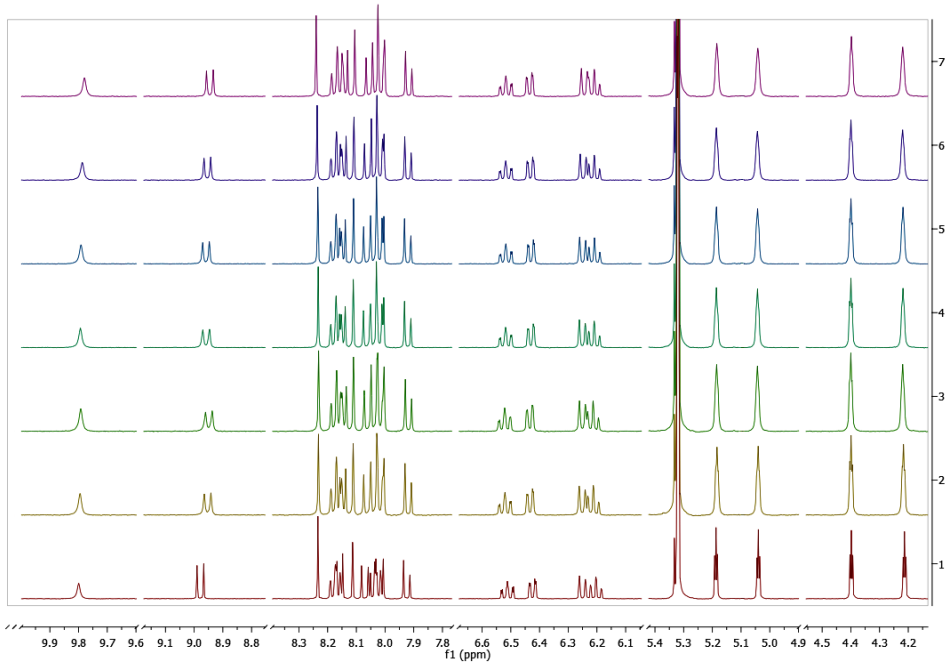

Figure S21. Evolution of the ^{1}H-NMR spectra of **1** (CD_2Cl_2, $c = 3 \cdot 10^{-3}$ M) in the presence of increasing amounts of Zn^{2+}.

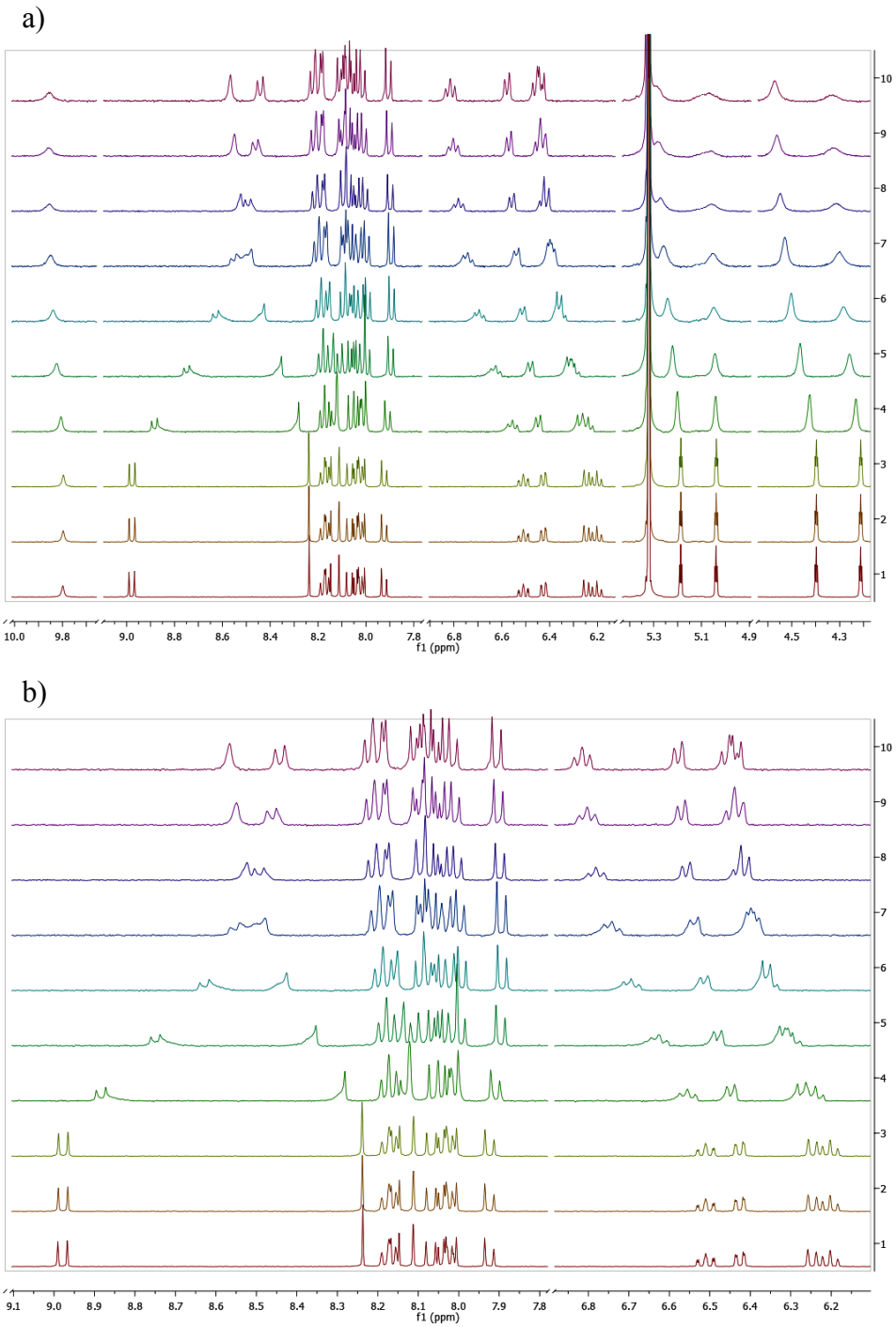

Figure S22. a) Evolution of the ^{1}H NMR spectrum of the previously formed [**1**·$H_2PO_4^-$] complex, upon addition of increasing amounts of Zn^{2+} from 0 (bottom) to 5 equiv (top); b) aromatic region of the spectra.

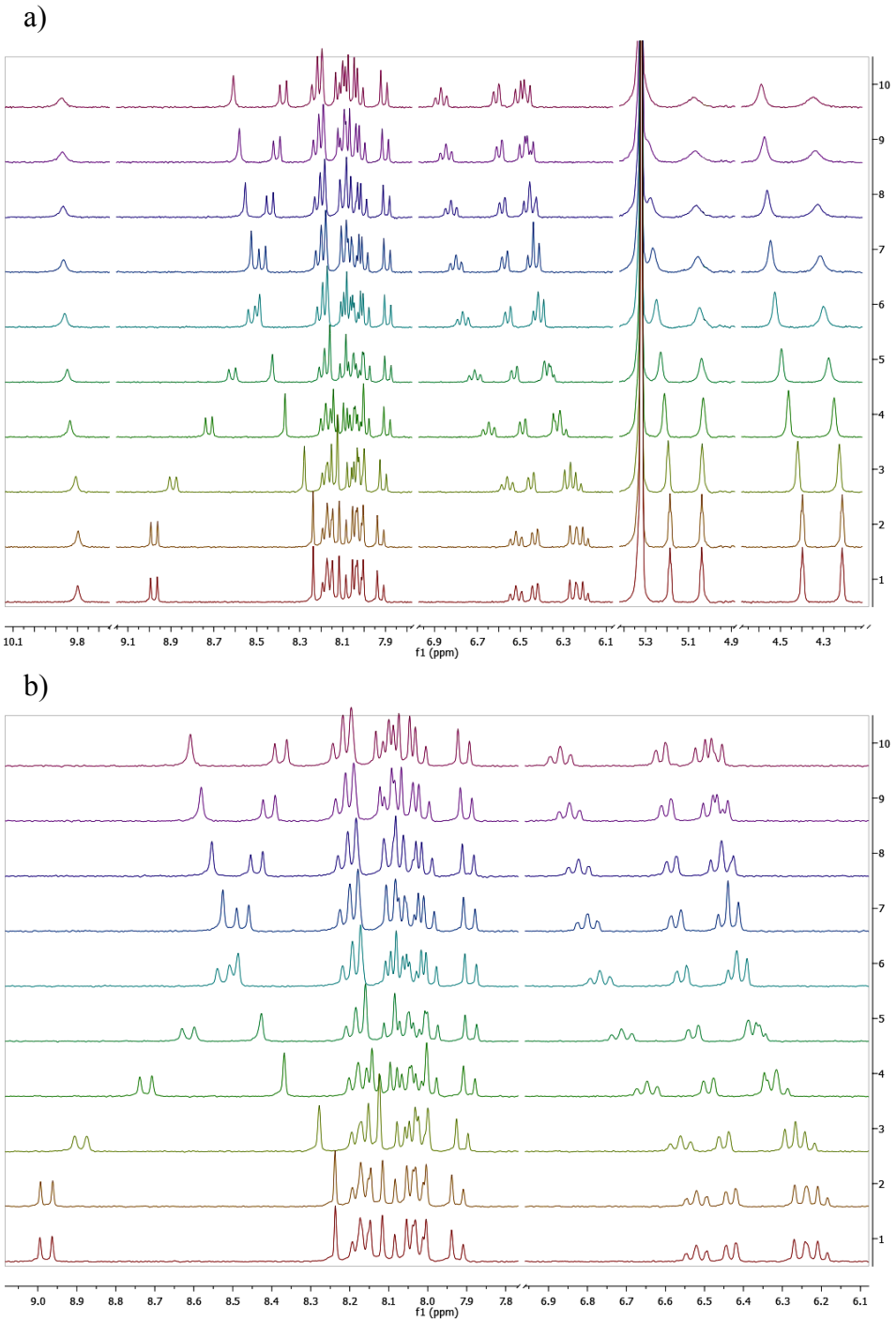

Figure S23. a) Variation of the ^{1}H NMR spectrum of the previously formed [**1**·$H_2PO_4^-$] complex, upon addition of increasing amounts of Cd^{2+} from 0 (bottom) to 4 equiv (top); b) aromatic region of the spectra.

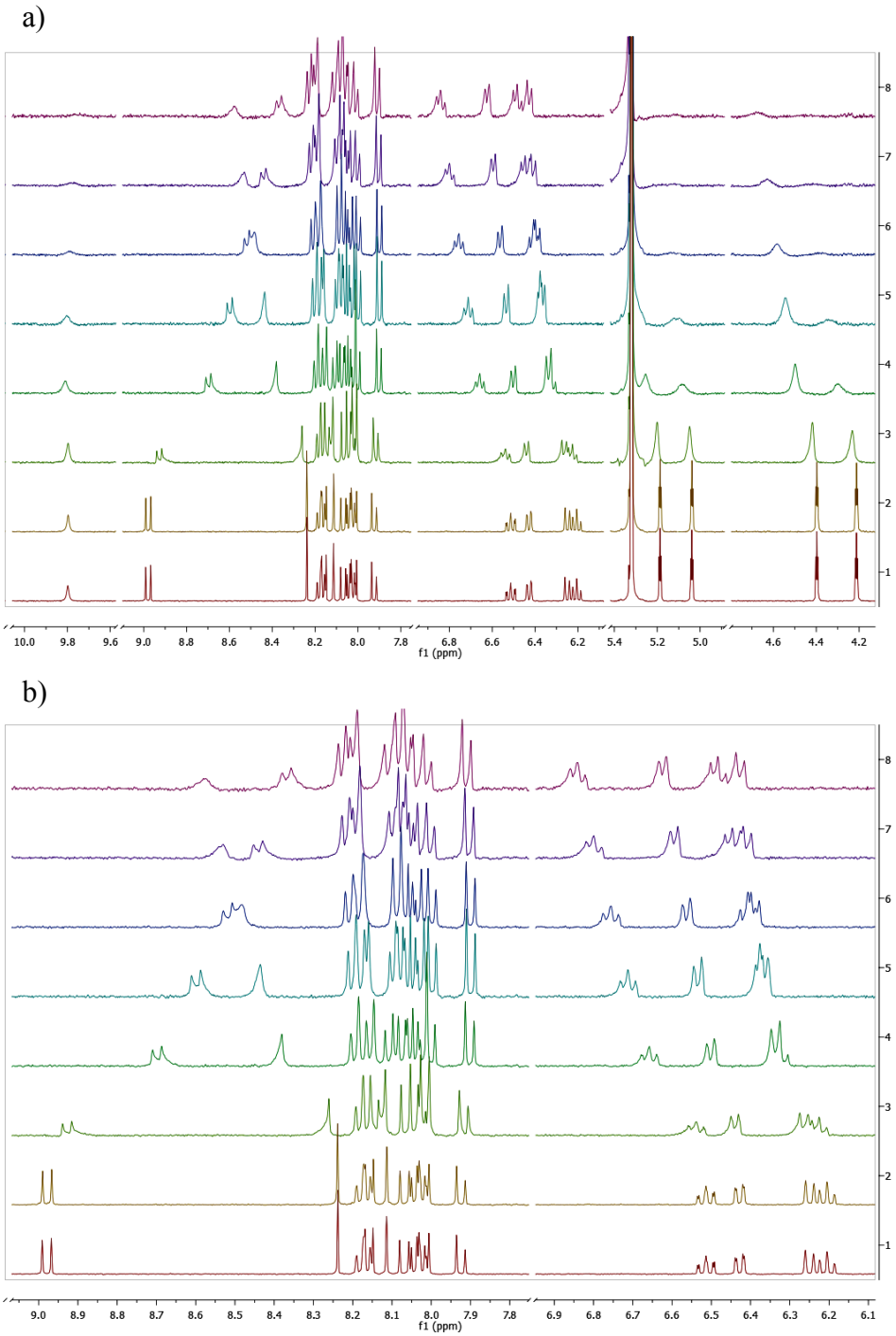

Figure S24. a) Evolution of the ^{1}H NMR spectrum of the previously formed [**1**·$H_2PO_4^-$] complex, upon addition of increasing amounts of Ca^{2+} from 0 (bottom) to 3 equiv (top); b) aromatic region of the spectra.

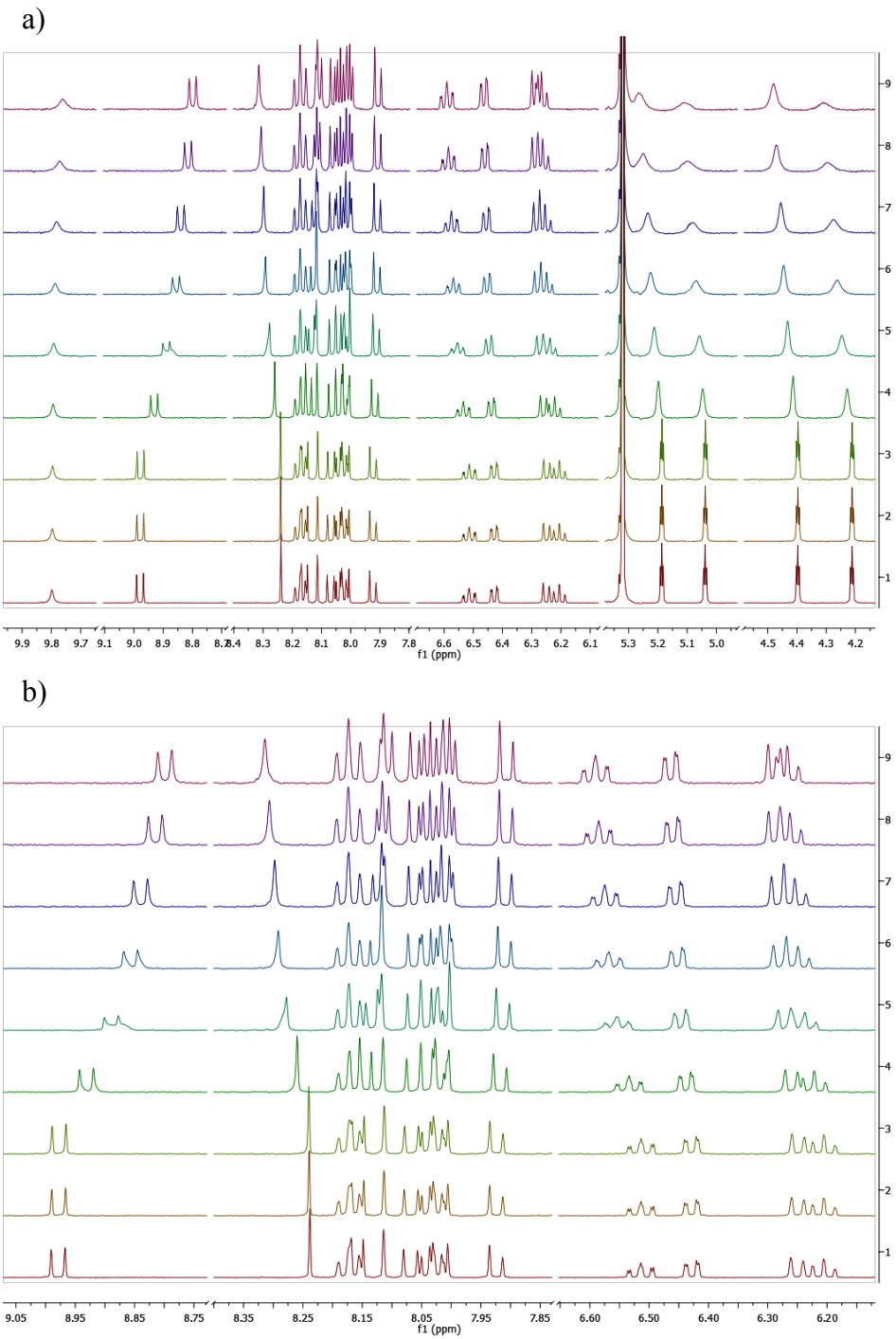

Figure S25. a) Variation of the ^{1}H NMR spectrum of the previously formed [**1**·$H_2PO_4^-$] complex, upon addition of increasing amounts of Mg^{2+} from 0 (bottom) to 6 equiv (top); b) aromatic region of the spectra.

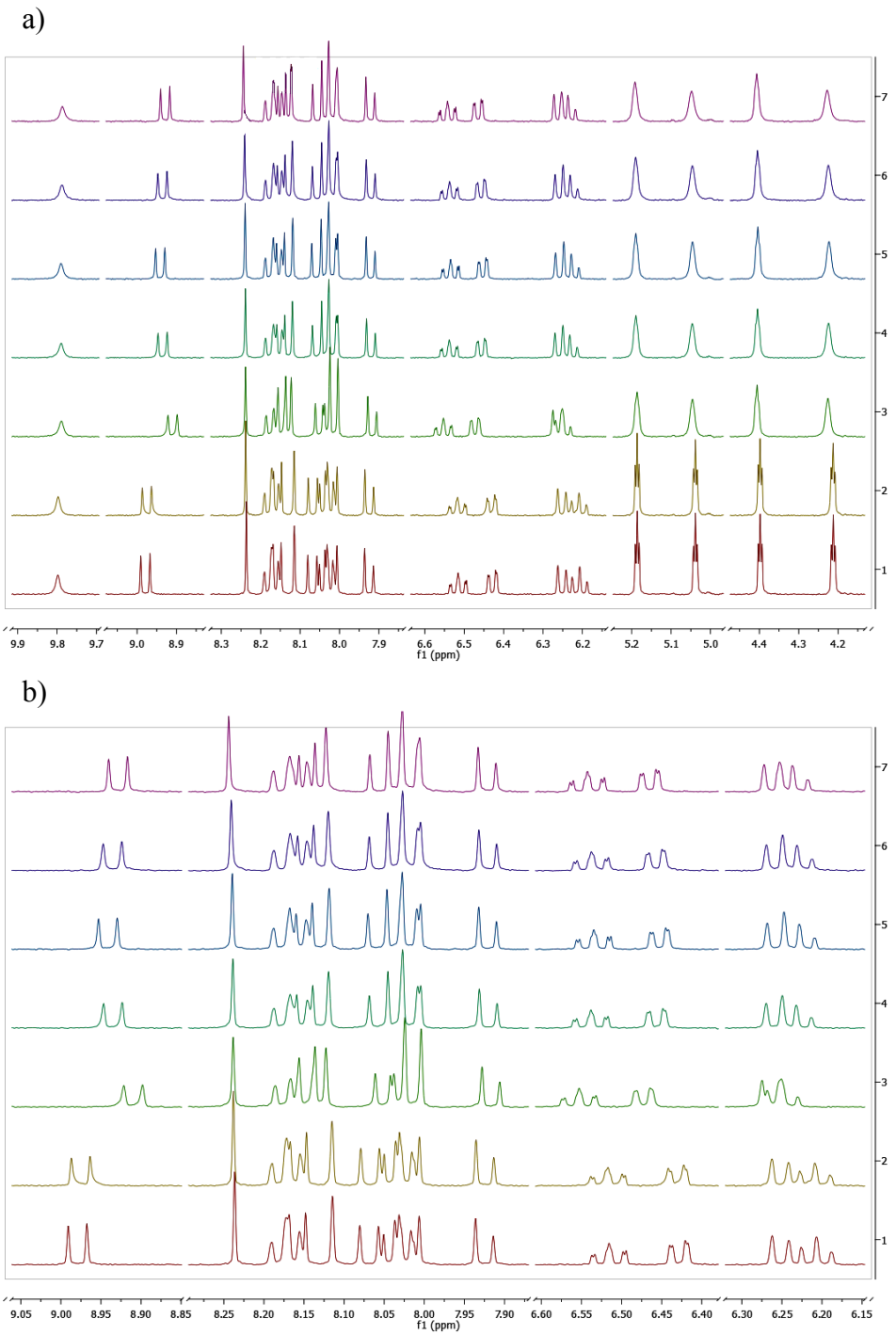

Figure S26. a) Evolution of the ^{1}H NMR spectrum of the previously formed [**1**·AcO^{-}] complex, upon addition of increasing amounts of Zn^{2+} from 0 (bottom) to 4 equiv (top); b) aromatic region of the spectra.

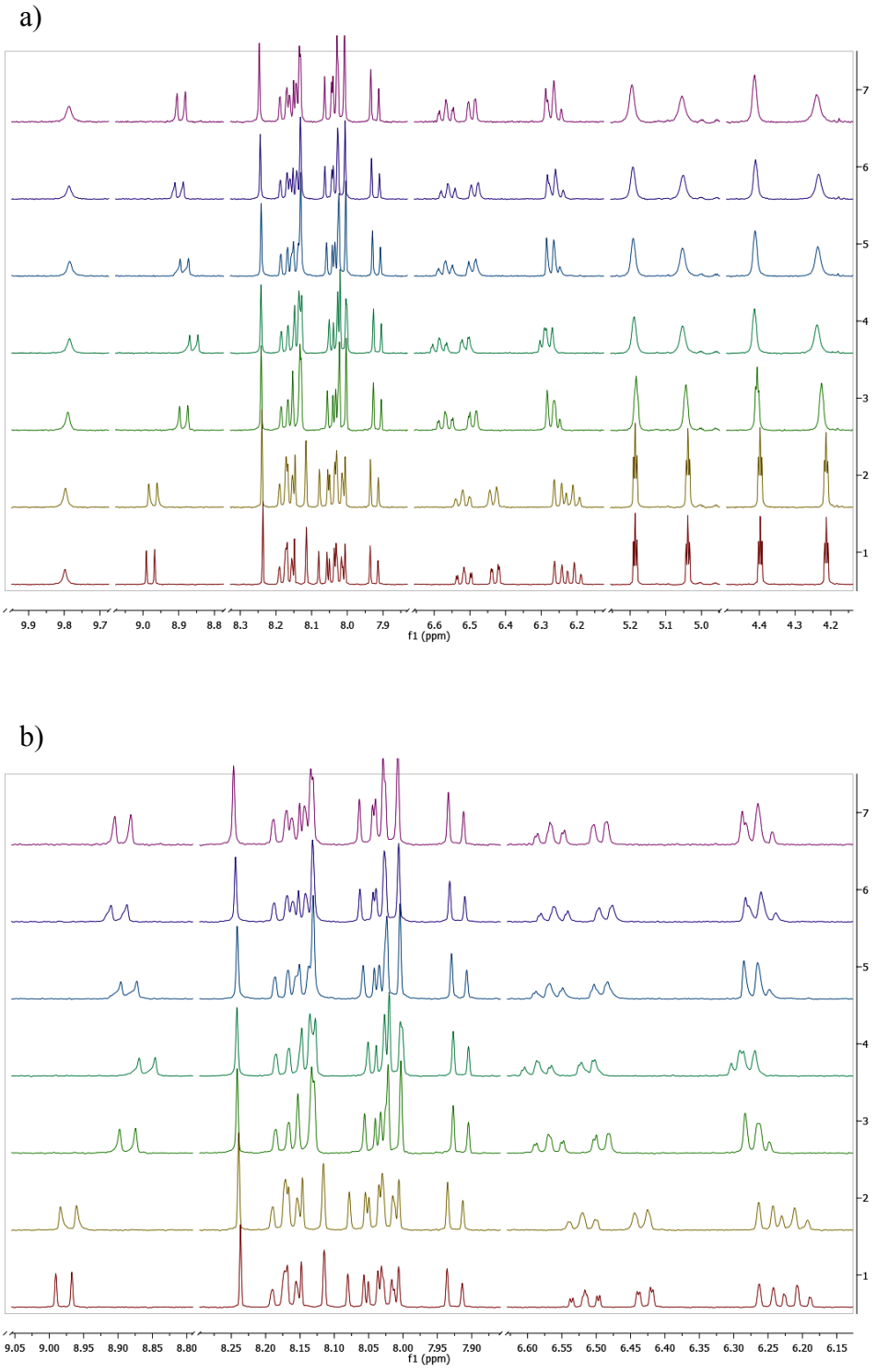

Figure S27. a) Variation of the ^{1}H NMR spectrum of the previously formed [**1**·AcO^{-}] complex, upon addition of increasing amounts of Cd^{2+} from 0 (bottom) to 4 equiv (top); b) aromatic region of the spectra.

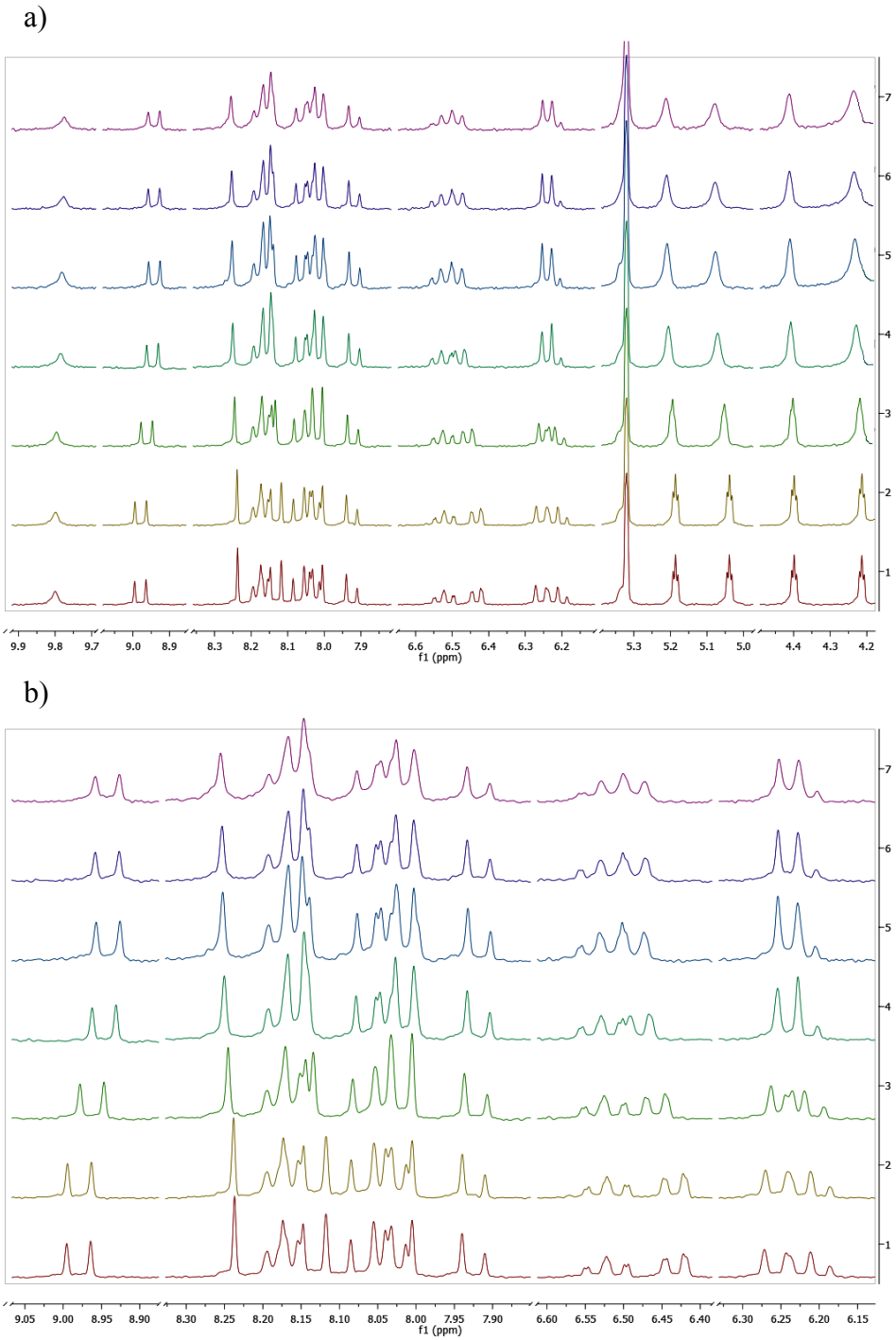

Figure S28. a) Evolution of the ^{1}H NMR spectrum of the previously formed [**1**·AcO^{-}] complex, upon addition of increasing amounts of Ca^{2+} from 0 (bottom) to 4 equiv (top); b) aromatic region of the spectra.

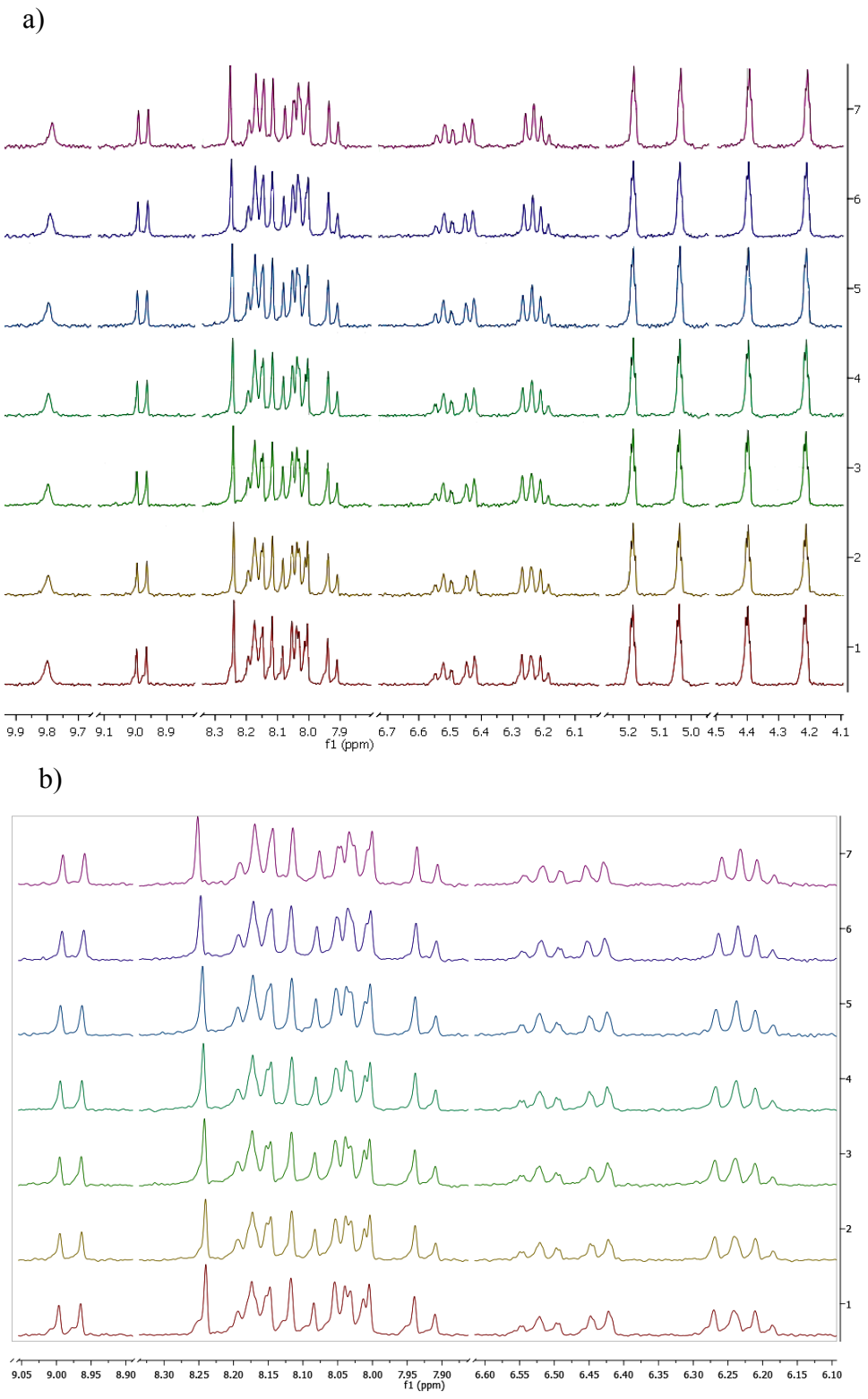

Figure S29. a) Evolution of the ^{1}H NMR spectrum of the previously formed [**1**·AcO^{-}] complex, upon addition of increasing amounts of Mg^{2+} from 0 (bottom) to 5 equiv (top); b) aromatic region of the spectra.

	H_{13}(amide)			H_{24}(pyrene)			H_{17}(triazole)			H_{41}(coumarin)		
	δ_i	δ_f	$\Delta\delta$	δ_i	δ_f	$\Delta\delta$	δ_i	δ_f	$\Delta\delta$	δ_i	δ_f	$\Delta\delta$
$[\mathbf{1}\cdot H_2PO_4\cdot Zn]^+$	9.80	9.86	0.06	8.98	8.44	-0.54	8.24	8.57	0.33	8.11	8.18	0.07
$[\mathbf{1}\cdot H_2PO_4\cdot Cd]^+$		9.88	0.08		8.38	-0.60		8.60	0.36		8.19	0.08
$[\mathbf{1}\cdot H_2PO_4\cdot Ca]^+$		9.75	-0.05		8.37	-0.61		8.58	0.34		8.19	0.08
$[\mathbf{1}\cdot H_2PO_4\cdot Mg]^+$		9.76	-0.04		8.80	-0.18		8.31	0.07		8.11	0
$[\mathbf{1}\cdot AcO\cdot Zn]^+$	9.80	9.79	-0.01	8.98	8.93	-0.05	8.24	8.25	0.01	8.11	8.12	0.01
$[\mathbf{1}\cdot AcO\cdot Cd]^+$		9.79	-0.01		8.89	0		8.25	0.01		8.13	0.02
$[\mathbf{1}\cdot AcO\cdot Ca]^+$		9.77	-0.03		8.94	-0.04		8.25	0.01		8.15	0.04
$[\mathbf{1}\cdot AcO\cdot Mg]^+$		9.79	-0.01		8.97	-0.01		8.25	0.01		8.11	0

	H_{44}(coumarin)			H_{42}(coumarin)			H_{45}(coumarin)			H_{43}(coumarin)		
	δ_i	δ_f	$\Delta\delta$	δ_i	δ_f	$\Delta\delta$	δ_i	δ_f	$\Delta\delta$	δ_i	δ_f	$\Delta\delta$
$[\mathbf{1}\cdot H_2PO_4\cdot Zn]^+$	6.51	6.82	0.31	6.43	6.58	0.15	6.25	6.43	0.18	6.20	6.45	0.25
$[\mathbf{1}\cdot H_2PO_4\cdot Cd]^+$		6.87	0.36		6.61	0.18		6.47	0.22		6.49	0.29
$[\mathbf{1}\cdot H_2PO_4\cdot Ca]^+$		6.84	0.33		6.62	0.19		6.43	0.18		6.48	0.28
$[\mathbf{1}\cdot H_2PO_4\cdot Mg]^+$		6.59	0.08		6.46	0.03		6.29	0.04		6.27	0.07
$[\mathbf{1}\cdot AcO\cdot Zn]^+$	6.52	6.54	0.02	6.43	6.47	0.05	6.25	6.26	0.01	6.21	6.24	0.03
$[\mathbf{1}\cdot AcO\cdot Cd]^+$		6.57	0.05		6.49	0.06		6.28	0.03		6.26	0.05
$[\mathbf{1}\cdot AcO\cdot Ca]^+$		6.50	-0.02		6.52	0.09		6.24	-0.01		6.23	0.02
$[\mathbf{1}\cdot AcO\cdot Mg]^+$		6.51	-0.01		6.44	0.01		6.25	0		6.21	0

Table S1. ^{1}H-NMR titration data of $[\mathbf{1}\cdot H_2PO_4^-]$ and $[\mathbf{1}\cdot AcO^-]$ complexes in the presence of Zn^{2+}, Cd^{2+}, Ca^{2+} and Mg^{2+} cations.

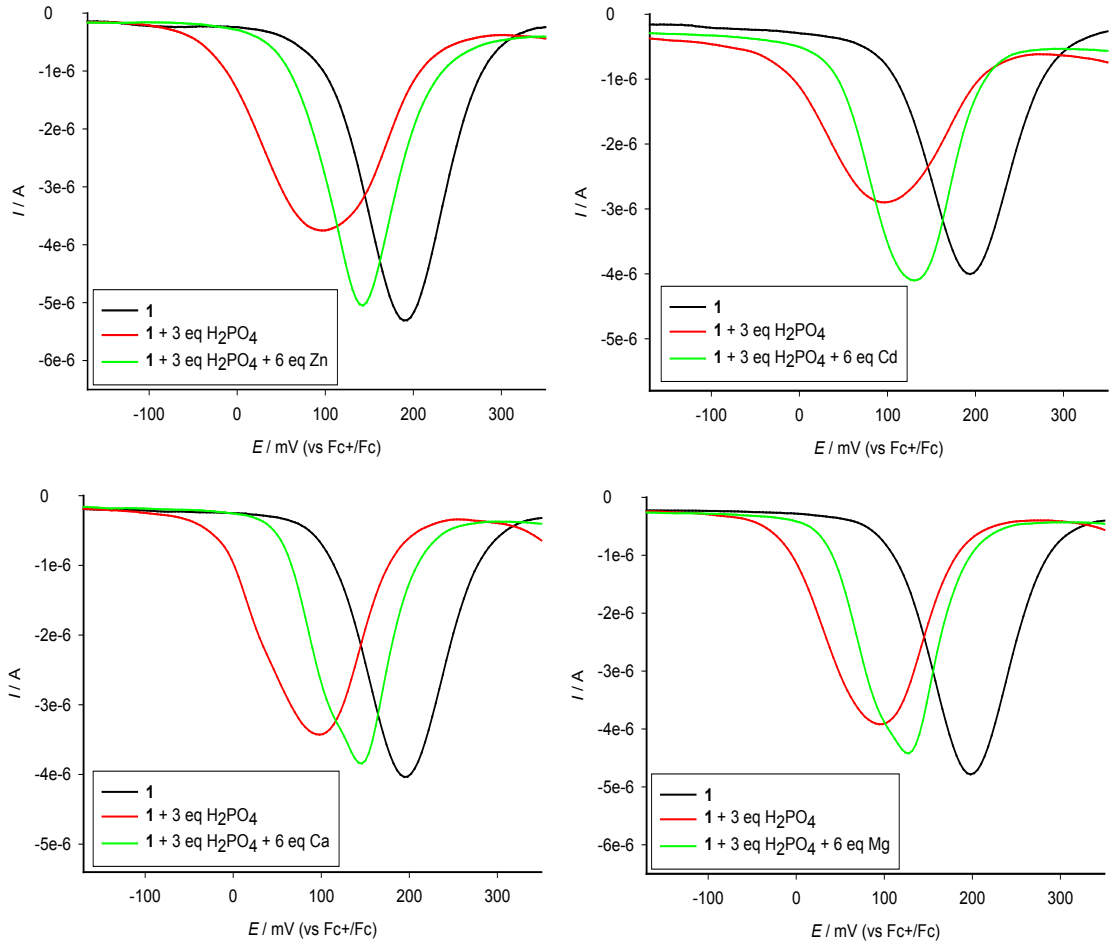

Figure S30. OSWV curves of the free receptor **1** in CH_3CN / CH_2Cl_2 (4:1, $c = 5 \cdot 10^{-4}$ M) (black) and the receptor with the addition of 3 equiv of $H_2PO_4^-$ (red), and with a mixture of both anion and cation (green) (supporting electrolyte, $c = 0.1$ M of TBAHP).

Compound	$E_{1/2}$ (mV)	$\Delta E_{1/2}$ (mV)
1	190	
[**1**·H_2PO_4]	095	
[**1**·H_2PO_4·Zn]$^+$	142	47
[**1**·H_2PO_4·Cd]$^+$	125	30
[**1**·H_2PO_4·Ca]$^+$	143	48
[**1**·H_2PO_4·Mg]$^+$	124	29

Table S2. Electrochemical data of the receptor **1** in the presence of $H_2PO_4^-$ and Zn^{2+}, Cd^{2+}, Ca^{2+} and Mg^{2+}.

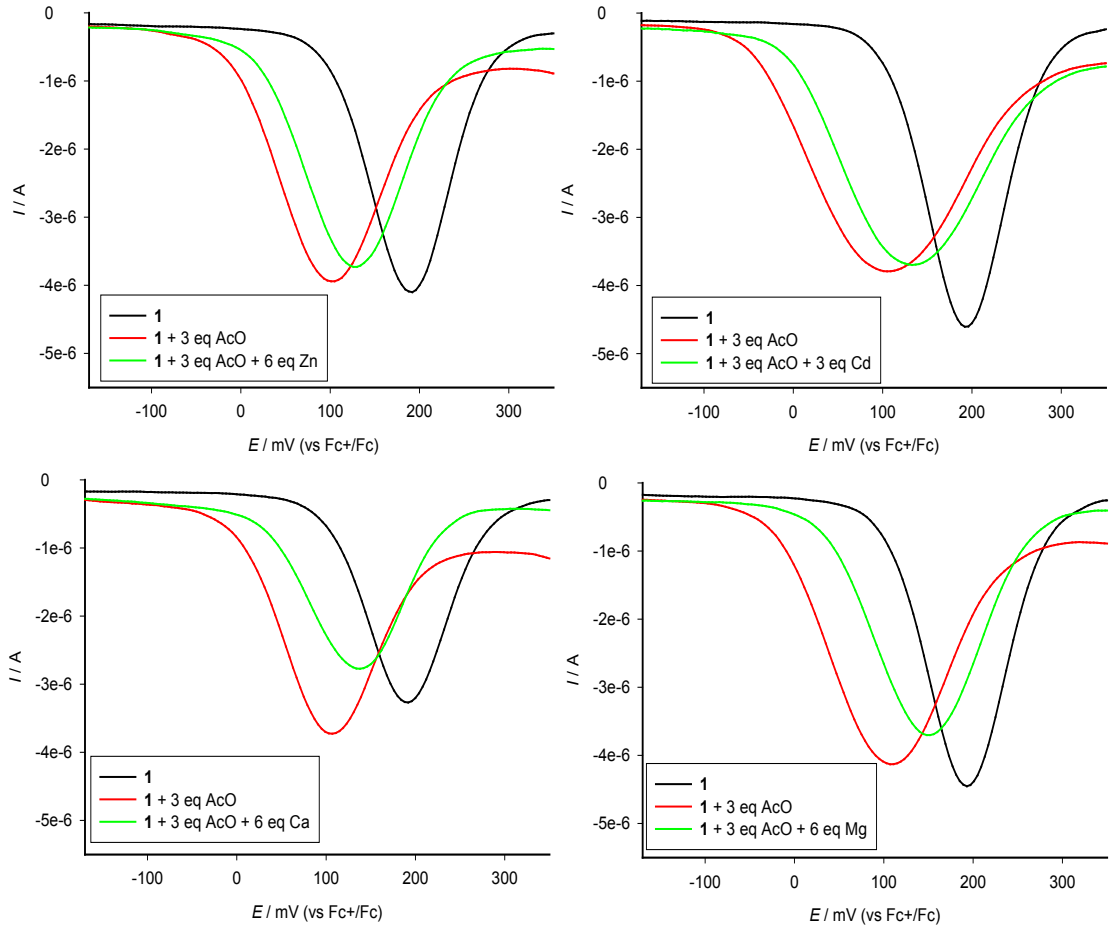

Figure S31. OSWV curves of the free receptor **1** in CH_3CN / CH_2Cl_2 (4:1, $c = 5 \cdot 10^{-4}$ M) (black) and the receptor with the addition of 3 equiv of AcO^- (red), and with a mixture of both anion and cation (green) (supporting electrolyte, c = 0.1 M of TBAHP).

Compound	$E_{1/2}$ (mV)	$\Delta E_{1/2}$ (mV)
1	190	
[**1**·AcO]	102	
$[\mathbf{1}\cdot AcO\cdot Zn]^+$	126	24
$[\mathbf{1}\cdot AcO\cdot Cd]^+$	129	27
$[\mathbf{1}\cdot AcO\cdot Ca]^+$	134	32
$[\mathbf{1}\cdot AcO\cdot Mg]^+$	144	42

Table S3. Electrochemical data of the receptor **1** in the presence of AcO^- and Zn^{2+}, Cd^{2+}, Ca^{2+} and Mg^{2+}.

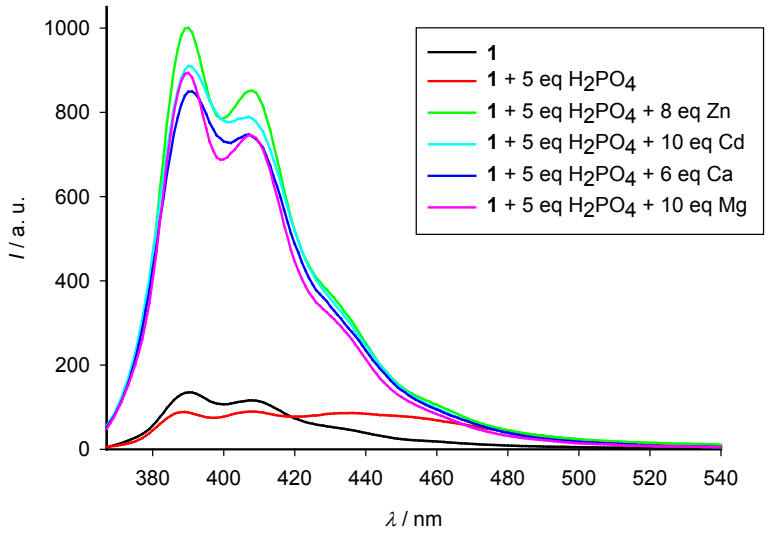

Figure S32. Evolution of the emission of the free receptor **1** in CH_3CN / CH_2Cl_2 (4:1, $c = 1.5 \cdot 10^{-5}$ M) (black), upon addition of 5 equiv of $H_2PO_4^-$ (red); initial addition of $H_2PO_4^-$ followed by addition of Zn^{2+} (green), Cd^{2+} (blue), Ca^{2+} (dark blue) and Mg^{2+} (violet).

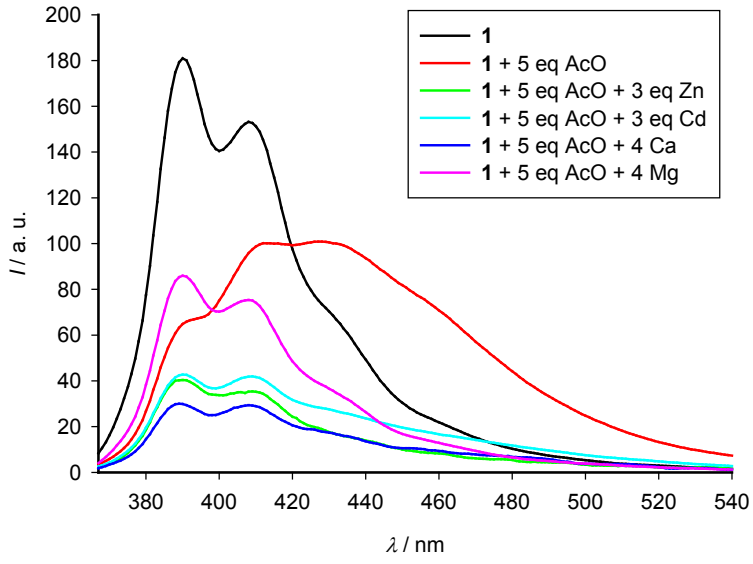

Figure S33. Evolution of the emission of the free receptor **1** in CH_3CN / CH_2Cl_2 (4:1, $c = 1.5 \cdot 10^{-5}$ M) (black), upon addition of 5 equiv of AcO^- (red); initial addition of AcO^- followed by addition of Zn^{2+} (green), Cd^{2+} (blue), Ca^{2+} (dark blue) and Mg^{2+} (violet).

Compound	Φ
1	0.008
[**1**·H_2PO_4]	0.010
[**1**·H_2PO_4·Zn]$^+$	0.070
[**1**·H_2PO_4·Cd]$^+$	0.051
[**1**·H_2PO_4·Ca]$^+$	0.050
[**1**·H_2PO_4·Mg]$^+$	0.046
[**1**·AcO]	0.009
[**1**·AcO·Zn]$^+$	0.003
[**1**·AcO·Cd]$^+$	0.004
[**1**·AcO·Ca]$^+$	0.002
[**1**·AcO·Mg]$^+$	0.005

Table S4. Quantum yield values of the receptor **1** and the different complexes formed with $H_2PO_4^-$ and AcO^- anions and Zn^{2+}, Cd^{2+}, Ca^{2+} and Mg^{2+}.cations.

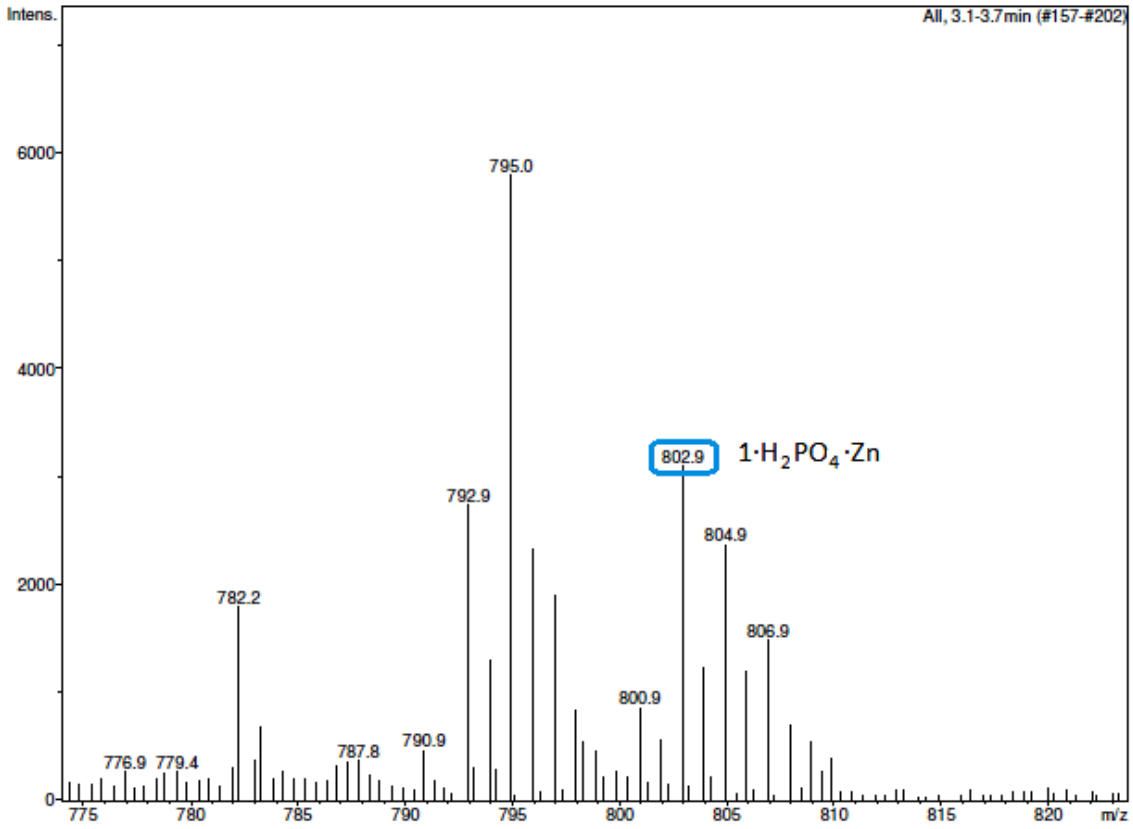

Figure S34. Positive ESI-MS spectrum of compound **1** with 1 equiv of $H_2PO_4^-$ and 2 equiv of Zn^{2+}. Peak at 802 m/z corresponds to the 1:1:1 complex.

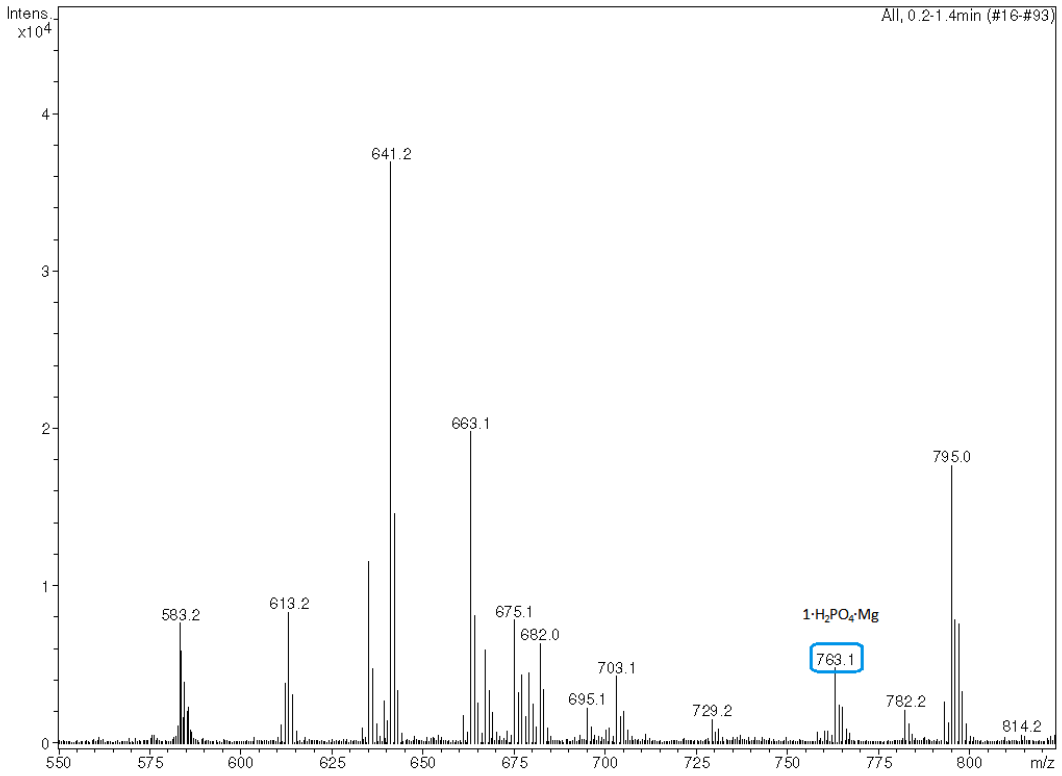

Figure S35. Positive ESI-MS spectrum of compound **1** with 1 equiv of $H_2PO_4^-$ and 2 equiv of Mg^{2+}. Peak at 763 m/z corresponds to the 1:1:1 complex.

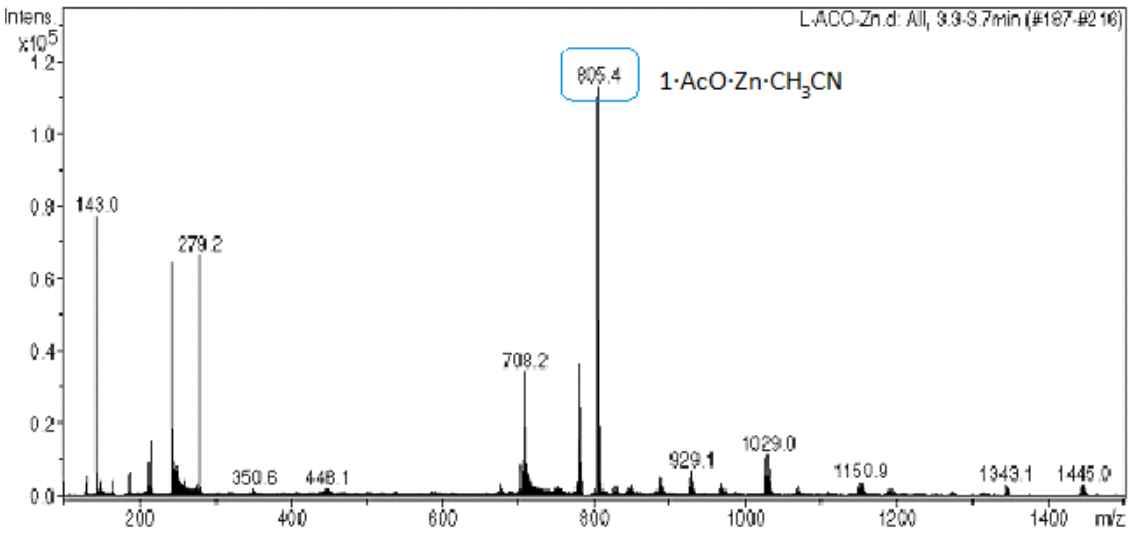

Figure S36. Positive ESI-MS spectrum of compound **1** with 1 equiv of AcO^- and 2 equiv of Zn^{2+}. Peak at 805 m/z corresponds to the 1:1:1 complex and a CH_3CN molecule.

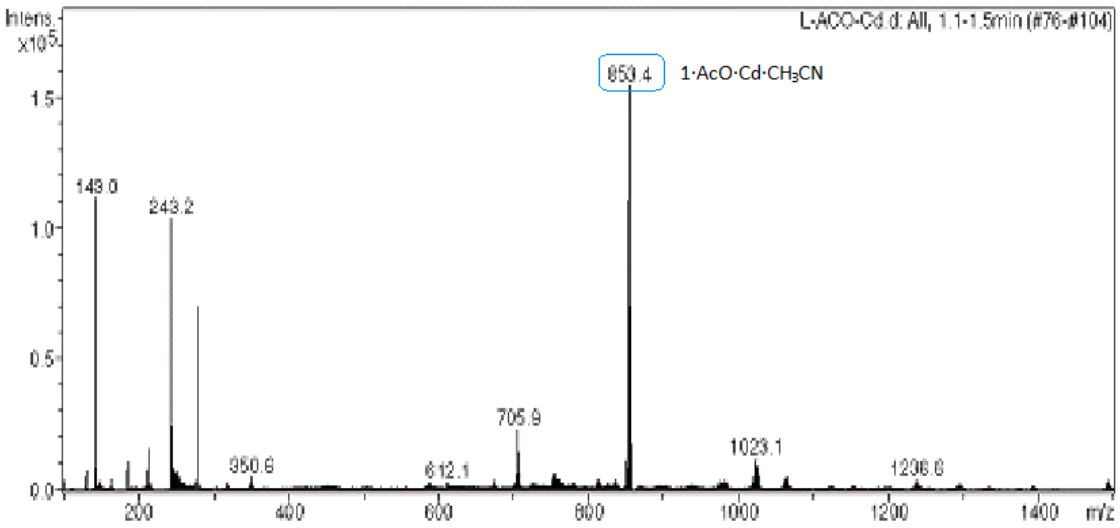

Figure S37. Positive ESI-MS spectrum of compound **1** with 1 equiv of AcO^- and 2 equiv of Cd^{2+}. Peak at 853 m/z corresponds to the 1:1:1 complex and a CH_3CN molecule.

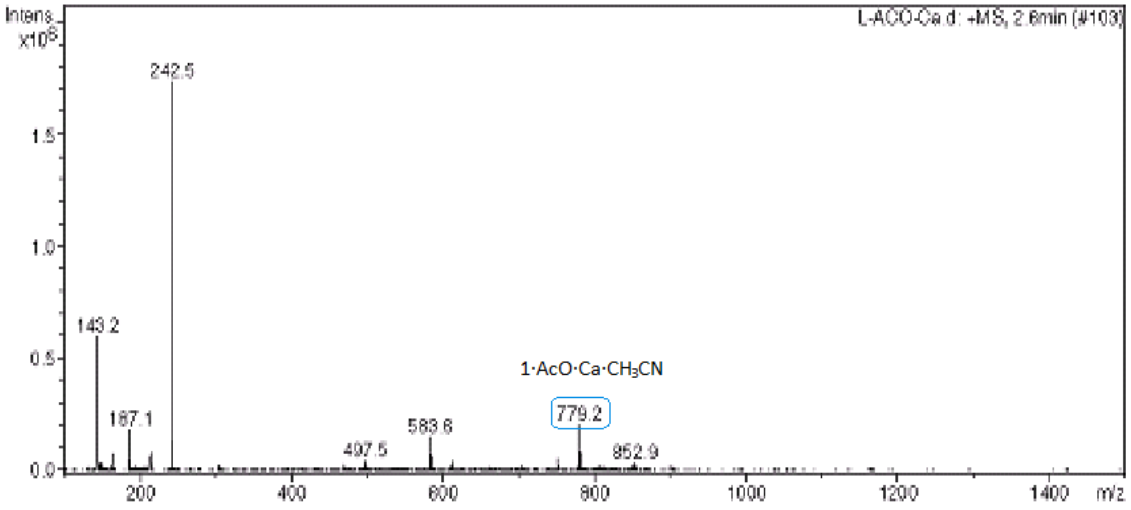

Figure S38. Positive ESI-MS spectrum of compound **1** with 1 equiv of AcO^- and 2 equiv of Ca^{2+}. Peak at 779 m/z corresponds to the 1:1:1 complex and a CH_3CN molecule.

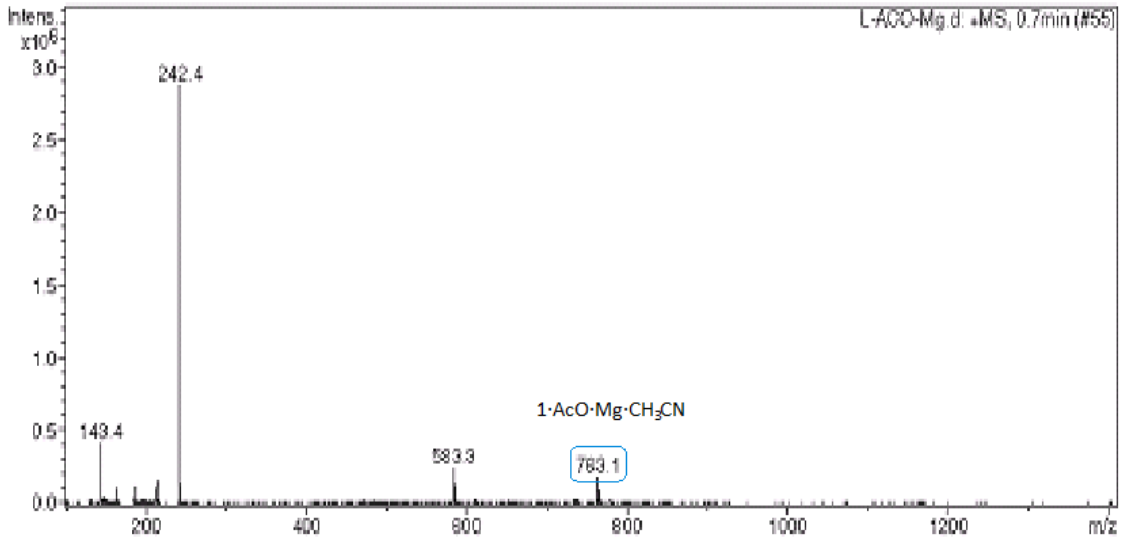

Figure S39. Positive ESI-MS spectrum of compound **1** with 1 equiv of AcO^- and 2 equiv of Mg^{2+}. Peak at 763 m/z corresponds to the 1:1:1 complex and a CH_3CN molecule.

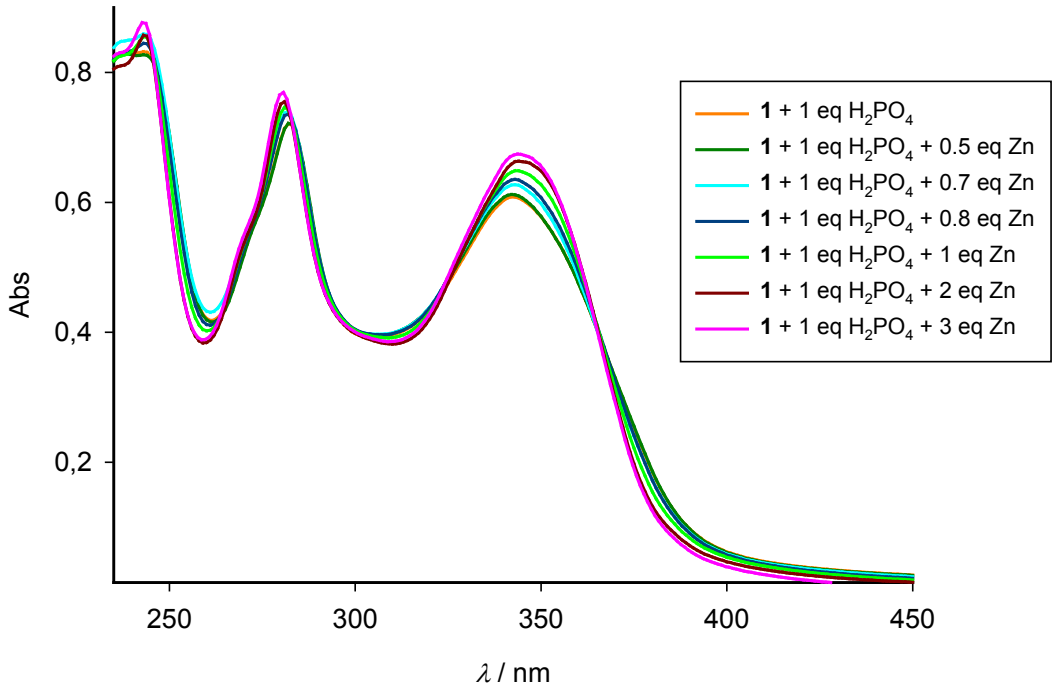

Figure S40. Changes in the absorption spectra of the previously formed [**1**·$H_2PO_4^-$] complex upon addition of increasing amounts of Zn^{2+} from 0 to 3 equiv.

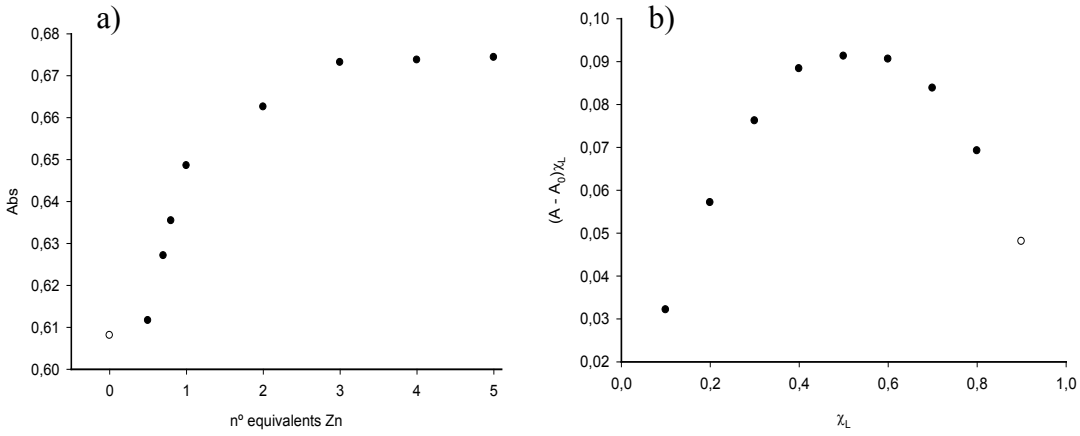

Figure S41. Binding profile of the titration of the [**1**·$H_2PO_4^-$] complex upon addition of increasing amounts of Zn^{2+} in CH_3CN / CH_2Cl_2 (4:1, c = $3\cdot10^{-5}$ M) measured at 345 nm. b) Job´s plot showing a 1:1 stoichiometry. The total [**1**·$H_2PO_4^-$] + [Zn^{2+}] = $3\cdot10^{-5}$ M.

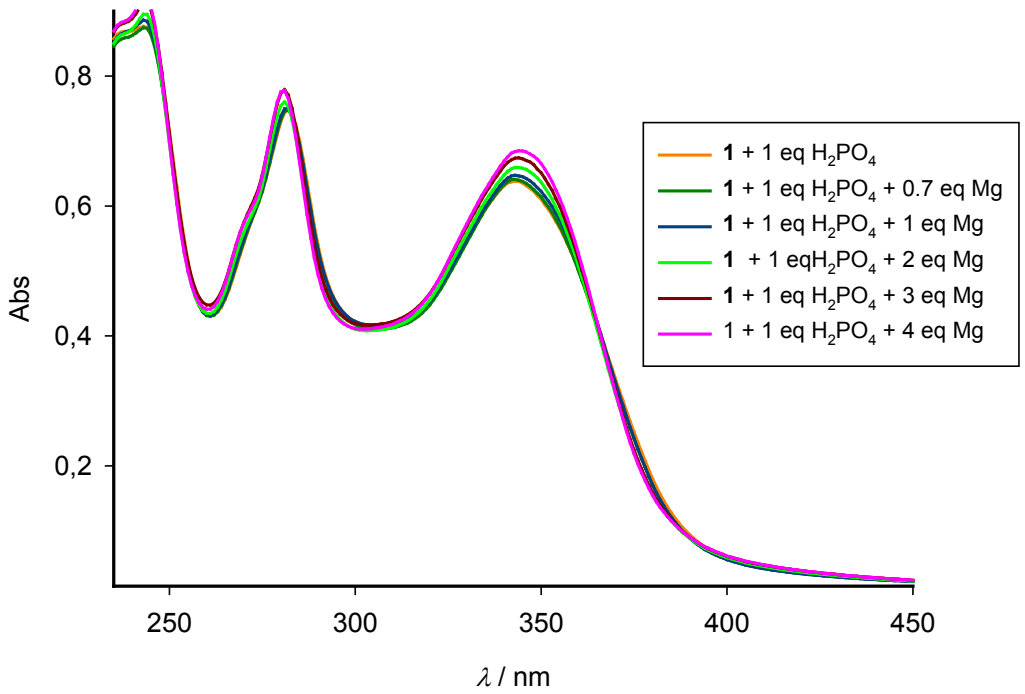

Figure S42. Changes in the absorption spectra of the previously formed [**1**·$H_2PO_4^-$] complex upon addition of increasing amounts of Mg^{2+} from 0 to 4 equiv.

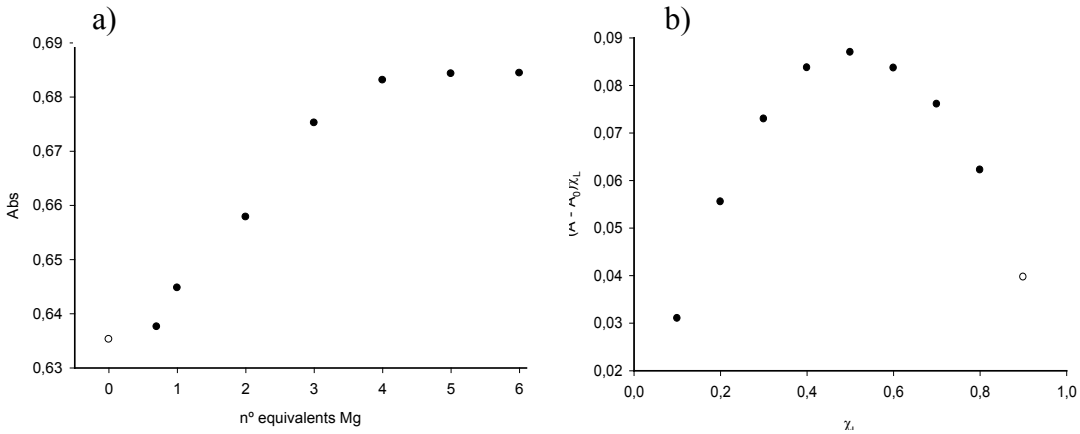

Figure S43. Binding profile of the titration of the [**1**·$H_2PO_4^-$] complex upon addition of increasing amounts of Mg^{2+} in CH_3CN / CH_2Cl_2 (4:1, $c = 3\cdot10^{-5}$ M) measured at 345 nm. b) Job´s plot showing a 1:1 stoichiometry. The total [**1**·$H_2PO_4^-$] + [Mg^{2+}] = $3\cdot10^{-5}$ M.

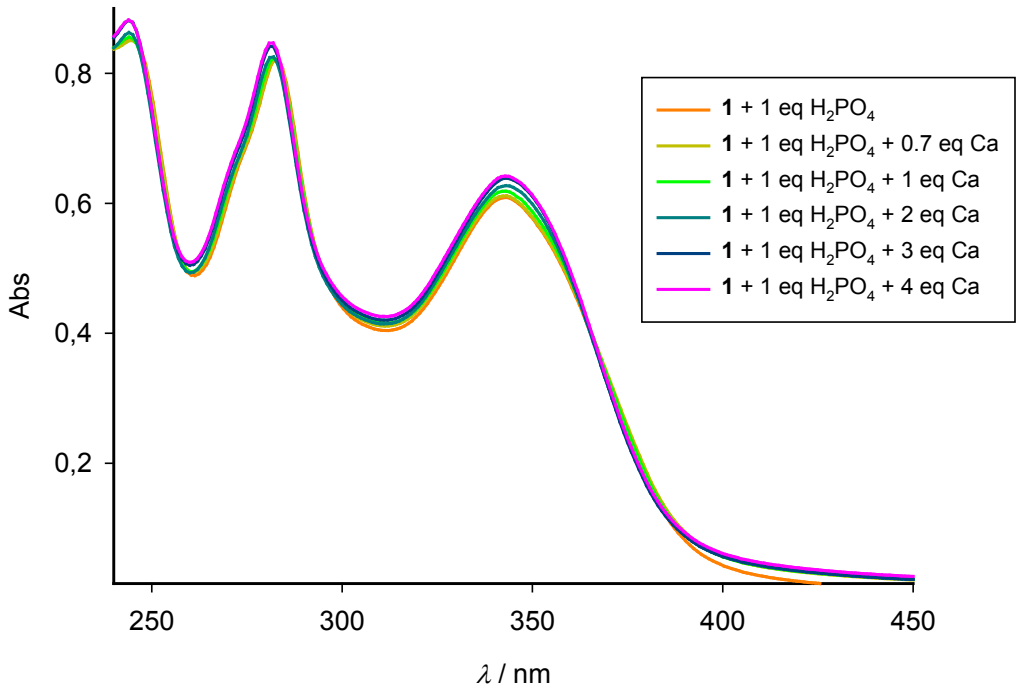

Figure S44. Changes in the absorption spectra of the previously formed [**1**·$H_2PO_4^-$] complex upon addition of increasing amounts of Ca^{2+} from 0 to 4 equiv.

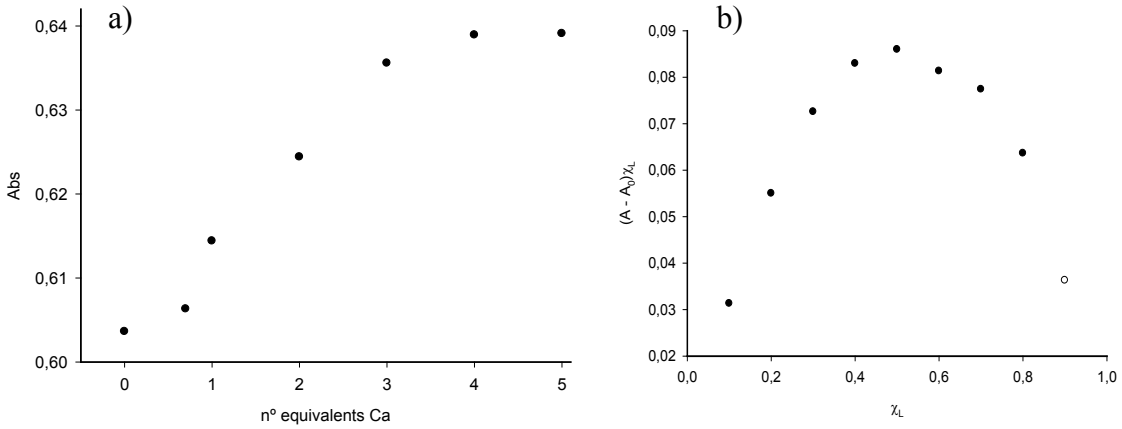

Figure S45. Binding profile of the titration of the [**1**·$H_2PO_4^-$] complex upon addition of increasing amounts of Ca^{2+} in CH_3CN / CH_2Cl_2 (4:1, $c = 3 \cdot 10^{-5}$ M) measured at 345 nm. b) Job´s plot showing a 1:1 stoichiometry. The total [**1**·$H_2PO_4^-$] + [Ca^{2+}] = $3 \cdot 10^{-5}$ M.

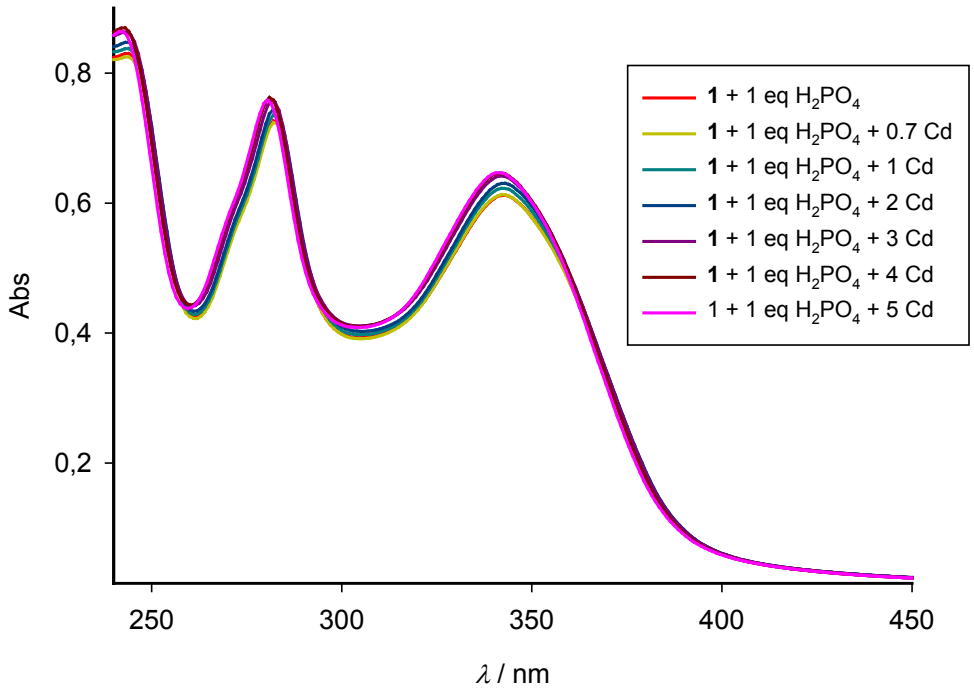

Figure S46. Changes in the absorption spectra of the previously formed [**1**·$H_2PO_4^-$] complex upon addition of increasing amounts of Cd^{2+} from 0 to 5 equiv.

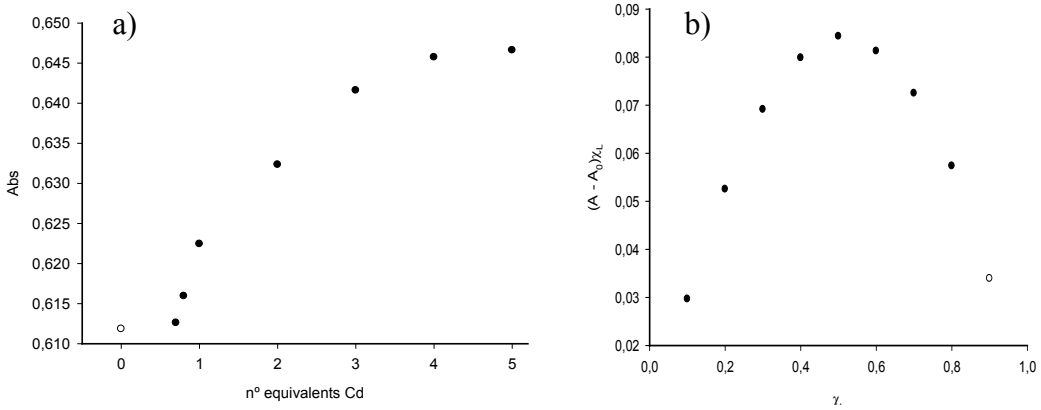

Figure S47. Binding profile of the titration of the [**1**·$H_2PO_4^-$] complex upon addition of increasing amounts of Cd^{2+} in CH_3CN / CH_2Cl_2 (4:1, $c = 3 \cdot 10^{-5}$ M) measured at 345

nm. b) Job´s plot showing a 1:1 stoichiometry. The total $[\mathbf{1}\cdot H_2PO_4^-] + [Cd^{2+}] = 3\cdot10^{-5}$ M.

Compound	K_{as} (M^{-1})	Error (M^{-1})
$[\mathbf{1}\cdot H_2PO_4\cdot Zn]^+$	$3.1x10^4$	$\pm 1.2x10^3$
$[\mathbf{1}\cdot H_2PO_4\cdot Cd]^+$	$4.5x10^4$	$\pm 4.0x10^3$
$[\mathbf{1}\cdot H_2PO_4\cdot Ca]^+$	$2.8x10^4$	$\pm 1.1x10^3$
$[\mathbf{1}\cdot H_2PO_4\cdot Mg]^+$	$5.6x10^4$	$\pm 3.9x10^3$

Table S5. Binding constants of the different complexes formed with the receptor **1** and $H_2PO_4^-$ and Zn^{2+}, Cd^{2+}, Ca^{2+} and Mg^{2+}.cations.

Computed structure for the ligand 1

The structure of ligand **1** (Figure 4a in the main text) contains a rigid 3-coumarinylcarboxamido side-arm, due to strong internal H-bond ($d_{NH\cdots OC}$ = 1.881 Å; WBI 0.034; $\rho(r) = 3.30\cdot10^{-2}$ e/a_o^3), roughly coplanar with the ferrocenyl Cp group by virtue of an additional weaker $H_{Cp}\cdots O$ interaction (d = 2.409 Å; WBI 0.002; $\rho(r) = 1.34\cdot10^{-2}$ e/a_o^3). The other pyrenyl-triazolyl side-arm is located in a stacked conformation stabilized by parallel coumarine-pyrene π-stacking interaction,[13] as well as by week H-bonding between the amide carbonyl group and the triazolyl H17 atom ($d_{C=O\cdots H}$ = 2.612 Å; WBI 0.002; $\rho(r) = 0.80\cdot10^{-2}$ e/a_o^3). In total, the inter-arms stabilizing interactions in **1** can be estimated to be 12.00 kcal/mol by comparison with a second conformer $\mathbf{1}^{conf}$ lacking both of them. Furthermore, from the formamide model derivatives **2** and $\mathbf{2}^{conf}$ (not shown), built up by replacing the coumarine moiety by an appropriately located H atom in frozen geometries of **1** and $\mathbf{1}^{conf}$, the magnitude of the H-bonding was found to be of 1.82 kcal/mol, from which the π-stacking is estimated to amount to 10.18 kcal/mol.

Detailed description of the ^{1}H NMR titration with metals.

[13] Mean planes are separated 3.470 Å at the coumarine centroid, with interplanes angle 0.82°. Four BCPs (bond critical points) were found between both planes, featuring $\Sigma\rho(r) = 1.85\cdot10^{-2}$ e/a_o^3 and ΣWBI = 0.050 (extended to all coumarine-pyrene atom-atom pairwise interactions).

It is worth mentioning that during the formation of the ion-pair complex the most important shifts are the following: a) the NH proton is slightly downfield shifted; b) the H-24 of the pyrene (in red) is importantly upfield shifted ($\Delta\delta$ = 0.60 ppm); c) the triazole H-17 (in green) is, by contrast, significantly downfield shifted ($\Delta\delta$ = 0.35 ppm); d) the coumarin protons (in dark blue) are also downfield shifted. All these variations indicate that in the complex, the NH group forms a stronger hydrogen bond with the ClO_4^- anion. The downfield shift of the triazole proton is a consequence of both the coordination of the metal to one N atom of the ring and a hydrogen bond formed with the ClO_4^- anion. The coordination of the ion-pair also breaks the interaction of H-24 of the pyrene unit causing the observed upfield shift. The general downfield shifted of the protons of coumarin moiety are then caused for the coordination of the metal to the C=O group that increase the electron-withdrawing effect of carbonyl group. Thus. the observed variation of the NMR spectrum supports, in general, the proposed theoretical structures.